Surface kinetic model for isotopic and trace element fractionation during precipitation of calcite from aqueous solutions

Donald J. DePaolo

Earth Sciences Division
Lawrence Berkeley National Laboratory
Berkeley, CA 94720

Department of Earth and Planetary Science
University of California
Berkeley, CA 94720

October 2010

ABSTRACT

A surface reaction kinetic model is developed for predicting Ca isotope fractionation and metal/Ca ratios of calcite as a function of rate of precipitation from aqueous solution. The model is based on the requirements for dynamic equilibrium; i.e. proximity to equilibrium conditions is determined by the ratio of the net precipitation rate (R_p) to the gross forward precipitation rate (R_f), for conditions where ionic transport to the growing crystal surface is not rate-limiting. The value of R_p has been experimentally measured under varying conditions, but the magnitude of R_f is not generally known, and may depend on several factors. It is posited that, for systems with no trace constituents that alter the surface chemistry, R_f can be estimated from the bulk far-from-equilibrium dissolution rate of calcite (R_b or k_b), since at equilibrium $R_f = R_b$, and $R_p = 0$. Hence it can be inferred that $R_f \approx R_p + R_b$. The dissolution rate of pure calcite is measureable and is known to be a function of temperature and pH. At given temperature and pH, equilibrium precipitation is approached when R_p ($= R_f - R_b$) $<< R_b$. For precipitation rates high enough that $R_p >> R_b$, both isotopic and trace element partitioning are controlled by the kinetics of ion attachment to the mineral surface, which tend to favor more rapid incorporation of the light isotopes of Ca and discriminate weakly between trace metals and Ca. With varying precipitation rate, a transition region between equilibrium and kinetic control occurs near $R_p \approx R_b$ for Ca isotopic fractionation. According to this model, Ca isotopic data can be used to estimate R_f for calcite precipitation. Mechanistic models for calcite precipitation indicate that the molecular exchange rate is not constant at constant T and pH, but rather is dependent also on solution saturation state and hence R_p. Allowing R_b to vary as $R_p^{1/2}$, consistent with available precipitation rate studies, produces a better fit to some trace element and isotopic data than a model where R_b is constant. This model can account for most of the experimental data in the literature on the dependence of $^{44}Ca/^{40}Ca$ and metal/Ca fractionation in calcite as a function of precipitation rate and temperature, and also accounts for $^{18}O/^{16}O$ variations with some assumptions. The apparent temperature dependence of Ca isotope fractionation in calcite may stem from the dependence of R_b on temperature; there should be analogous *pH* dependence at $pH < 6$. The proposed model may be valuable for predicting the behavior of isotopic and trace element fractionation for

a range of elements of interest in low-temperature aqueous geochemistry. The theory presented is based on measureable thermo-kinetic parameters in contrast to models that require hyper-fast diffusivity in near-surface layers of the solid.

1. INTRODUCTION

Recent work on mid-mass stable isotope systems like Ca, Mg, Fe, Cr, and Mo suggests that minerals that form by precipitation from aqueous solution do not do so at isotopic equilibrium, especially when the precipitation is done at rates fast enough to be readily observed in laboratory experiments (Johnson et al., 2004). Furthermore, it has also been shown that in most instances the solid phase is enriched in the light isotope species relative to the solution phase. While some studies have suggested that these fractionations associated with precipitation from solution may represent isotopic equilibrium (e.g. Lemarchand et al., 2004), and the reports of temperature dependence of fractionations can be viewed as broadly consistent with this interpretation (e.g. Gussone et al., 2005), the precipitation rate dependence (Tang et al., 2008) and preference for the light isotopes in the solid phase (Skulan et al., 1997; Skulan and DePaolo, 1999) suggest that the fractionations are mostly kinetic in origin. The recent observations on mid-mass stable isotope systems have potentially important implications for all stable isotope and trace element studies. Deviations from equilibrium fractionation behavior are common, and a more complete understanding of their origins is critical to fully capitalizing on the potential of isotopic and trace element measurements to provide information on geochemical processes and paleoenvironment (e.g. Smith et al., 1979; Beck et al., 1992; Zachos et al., 2002; Marshall and McCulloch, 2002; Fantle and DePaolo, 2005; Eisenhauer et al., 2010; Coggon et al., 2010).

It is the purpose of this contribution to propose a framework to help understand the many, and partly contradictory observations on calcium isotopic fractionation that have been made thus far, and to help define the additional data needed to more fully understand isotopic fractionation during mineral precipitation. The proposed model also accounts for the essential features of the incorporation of Sr and Mn into calcite, although trace element

partitioning, as opposed to isotopic fractionation, is likely to require additional parameters to achieve a full description. The approach taken is one using a macroscopic treatment of chemical kinetics, and can be viewed as an extension of one component of the box model of Fantle and DePaolo (2007). It is expected that this macroscopic treatment can be extended to include a molecular scale description of the processes involved in mineral growth (e.g. Teng et al., 2000; DeYoreo et al., 2009; Morse et al., 2007), and how they relate to isotopic fractionation.

1.1. Surface reaction effects, transport-control, and isotopic equilibrium

The conditions necessary for isotopic equilibrium are analogous to those for chemical equilibrium. Chemical reactions are conceptualized as the net result of a forward and backward reaction. At equilibrium, the rate of the forward reaction (R_f) is balanced exactly by the rate of the backward reaction (R_b). Equilibrium can be maintained only through the rapid and continual exchange of material between reactant and product phases. In order for a reaction to proceed (such that the amounts of the product phases increase at the expense of the reactants) *at equilibrium* requires that the net reaction rate ($R_p = R_f - R_b$) be much smaller than either the gross forward or gross backward reaction rates. This requirement can be stated simply in the form $R_p << R_b$. This same requirement applies to isotopic equilibrium. It is also to be expected, because the zero-point vibrational energy and the mean molecular velocity of light isotopes are higher than those for heavy isotopes, that the rate constants for both the forward and backward reactions are greater for light isotopic species than for heavier isotopic species (e.g. O'Neil, 1986; Criss, 1999; Zeebe and Wolf-Gladrow, 2001).

The requirement that the net precipitation rate is small relative to the gross exchange fluxes is necessary but not sufficient to ensure equilibrium. It is also necessary that the net rate of reaction is small in comparison to the transport of reactants to the sites of reaction. Hence, the precipitation of minerals from solution can occur in at least four different regimes (Figure 1).

- In regime 1, the net precipitation rate is much slower than the gross exchange rates (R_f - R_b) << R_b, and slow enough that there are no transport limitations of ions to the surface of growing crystals. In this regime, which is restrictive, it can be expected that equilibrium will describe the isotopic and elemental fractionation between the aqueous species and solid phase.
- In regime 2, the net precipitation rate is much slower than the gross exchange rate, but fast enough that there are transport limitations in the fluid phase. In this case, it is a good approximation that the fluid phase *in contact with the crystal surface* is at or very near equilibrium with the crystal surface, but the solid is not growing in equilibrium with the bulk aqueous reservoir due to fractionation during transport (e.g. diffusion) of the aqueous species to the mineral surface. It is shown below that this condition is unlikely to be applicable to precipitation of calcite from aqueous solution.
- In regime 3, the net precipitation rate is larger than the gross exchange rate (R_f - R_b) ≥ R_b, but slow enough that there are no transport limitations in the fluid phase. In this case, the composition of the solid phase is determined mainly by the attachment-detachment kinetics of the species at the interface (i.e. surface reaction control), which means that the solid phase will tend to be *enriched in the light isotopic species*, in excess of whatever the equilibrium fractionation should be.
- In regime 4, the net precipitation rate is larger than the gross exchange rate and fast enough that there are also transport limitations in the fluid phase. This case is similar to regime 3, but the composition of the solid is affected by both attachment/detachment kinetics and mass transport in the fluid. Because light isotopic species will be transported faster, the solid phase will tend to be *enriched in the light isotopic species*, in excess of the equilibrium fractionation.

This qualitative summary of the relationships between fluid - mineral surface reaction kinetics provides a framework that is adequate to begin discussion of isotopic fractionation effects. It can be quantified further as discussed below, but may also need further modification to account for variations in reaction mechanism. This summary does not account for solid phase transport effects, which may affect the relationship between solid

and fluid phase isotopic composition under near-equilibrium (near-zero net crystal growth) conditions.

1.2. Examples of Regime 1 and Regime 2 condensation

Examples of precipitation (*sensu lato*) in regimes 1 and 2 with important isotopic fractionation consequences are provided by the condensation of water and ice from saturated and supersaturated air. An example of equilibrium, or near-equilibrium precipitation (Regime 1), is afforded by the condensation of water droplets from vapor-saturated air. Condensation occurs at very slight water vapor oversaturation values (< 1%), and the exchange fluxes at the liquid surface are >1000 times the net condensation flux. Regime 2 is illustrated by the condensation of ice crystals from vapor-oversaturated air in mixed (ice plus water droplets) clouds (Jouzel and Merlivat, 1984). Due to the co-existence of water vapor droplets and ice crystals, air in clouds can be oversaturated with respect to ice by 30% or more (Pruppacher and Klett, 1997; Libbrecht, 2005). At this level of oversaturation, the growth of ice crystals is limited by vapor phase transport of water molecules to the ice surface, the difference in vapor phase diffusivity between water isotope species has a large effect, and the ice crystals that form are enriched in light isotopes *relative to equilibrium values*. In this example, it is also the case that exchange at the ice surface between the solid and vapor is fast relative to the net condensation rate.

In the above mentioned examples of condensation of water from a gas phase, the exchange rate at the vapor-condensate interface can be estimated using the collision rate of water vapor molecules with the condensate surface (Knudsen, 1950; Hirschfelder et al., 1965; Richter, 2004), multiplied by a sticking coefficient (or accommodation coefficient, γ), as discussed in Pruppacher and Klett (1997) and Seinfeld and Pandis (1998). Although there is uncertainty in the accommodation coefficient, for water recent estimates place the value between 0.1 and 1 (Davidovits et al., 2004). Using a conservative value of 0.1, the implied exchange rate of molecules between saturated vapor and a liquid water surface is about R_b = 20 mol/m^2/sec at 25°C. A typical condensation rate (R_f - R_b) is about 0.003 mol/m^2/sec (for a 100 μm–radius droplet in 1% oversaturated air), about four orders of magnitude

smaller. The condensation flux varies as the inverse of the radius of the droplet, so indeed condensation of water droplets larger than 10 μm is expected to be a near-equilibrium process.

For ice at -15°C, the accommodation coefficient is estimated to be close to 1 (Libbrecht, 2005), and the implied exchange rate of molecules between the vapor and the ice surface is therefore 20 mol/m^2/sec (the higher value of γ is offset by lower temperature and lower saturation water vapor pressure). Ice condensation rates can be up to about 0.005 mol/m^2/sec (for a 100 μm–radius ice grain in 30% oversaturated air). The ice condensation rates are slow in comparison to the (theoretical) surface exchange rates, i.e. (R_f - R_b) << R_b, but they are fast enough, and occur at substantial vapor phase oversaturation and at low water vapor concentration, so that the growth is limited by diffusive transport of H_2O in the vapor phase. Hence ice condensation (or vapor deposition) occurs under conditions described by Regime 2. The kinetic isotopic effects associated with ice crystal growth in air can be simply described with a radial diffusion model because it can be assumed that the water vapor concentration in air at the ice surface is the equilibrium value (Jouzel and Merlivat, 1984; Seinfeld and Pandis, 1998). The kinetic effects cause large deviations from equilibrium (Figure 2) because the equilibrium fractionation favors the heavy isotopologue (e.g. $H_2{}^{18}O$) in the solid phase (α_{eq} = 1.018 at -15°C) whereas the diffusivity of the light isotopologue ($H_2{}^{16}O$) is larger in air so that the diffusive kinetic fractionation factor (D_{18}/D_{16} = 0. 972) is less than 1.

1.3. Equations for surface reaction control of $CaCO_3$ precipitation

The precipitation of minerals from aqueous solution is likely to occur in Regimes 3 and 4. However, as with the vapor phase condensation examples, the critical parameter is the exchange rate between fluid and mineral surface. For a vapor phase, the collision frequency can be calculated from kinetic theory. If the accommodation coefficient cannot be estimated, the exchange rate can be determined experimentally by evaporation into infinitely undersaturated vapor (or into vacuum) under conditions where there are no transport limitations (e.g. Richter, 2004). It is argued here, and this should be regarded as

a postulate that needs further proof, that the exchange rate for the mineral – aqueous fluid system can be measured experimentally as well, and is given by the mineral dissolution rate into a highly undersaturated solution under surface reaction controlled conditions (i.e. no transport limitations). This assumption is the initial thesis that is evaluated below. However, studies of calcite growth from aqueous solution strongly suggest that the surface exchange rate *is a function of saturation state of the solution*, which correlates with growth mechanism (e.g. Teng et al., 2000; DeYoreo et al., 2009). A second version of the model is also discussed where the surface exchange rate is allowed to be a function of oversaturation, with the functional form approximated based on experimental data on the relationship between calcite precipitation rates and solution oversaturation.

In the following section, equations describing Ca isotopic fractionation during calcite precipitation from aqueous solution are developed and then compared to recent experimental measurements. The available data fit the model well. This success has implications for the application of isotope ratio measurements to the understanding of mineral precipitation, and for understanding fluid-rock systems in nature. A key result is that experimentally measured *dissolution* rates can be used to infer whether mineral *precipitation* is likely to be occurring under near-equilibrium or kinetically controlled conditions.

The precipitation rate (R_f; the forward rate) and dissolution rate (R_b; backward rate) for calcite in a solution where pH ≥ 7.5 can be written in simplified form as (Lopez et al., 2009):

$$R_f = k_f \gamma_{Ca} \gamma_{CO_3} [Ca^{2+}]_{fs} [CO_3^{2-}]_{fs} = k_f^* [Ca^{2+}]_{fs} [CO_3^{2-}]_{fs} \quad (1a)$$

$$R_b = k_b [CaCO_3] \quad (1b)$$

where "*fs*" denotes the fluid at the mineral surface, k_f is the (forward) rate constant for precipitation and k_b is the (backward) rate constant for dissolution. The units of k_f and k_b depend on the units used for concentration. If the concentrations are expressed in

dimensionless units relative to a standard state (hypothetical 1 molal solution for aqueous species; pure $CaCO_3$ for the solid), then the units of k_f and k_b will be fluxes, such as mol/m^2/sec. At equilibrium the forward and backward rates are equal, and hence the equilibrium constant for the dissolution reaction is $K_{eq} = k_b/k'_f$ (cf. Lasaga, 1998).

It follows from equations 1a and 1b and the expression for K_{eq} that the *net* precipitation rate (R_p) can be written in the form:

$$R_p = R_f - R_b = k'_f \left([Ca^{2+}]_{fs}[CO_3^{2-}]_{fs} - [Ca^{2+}]_{eq}[CO_3^{2-}]_{eq} \right) \qquad (2a)$$

For the conditions prevalent in marine waters, namely $[Ca^{2+}] >> [CO_3^{2-}]$, this equation can be simplified to:

$$R_p = k'_f [Ca^{2+}]_{sol} \left([CO_3^{2-}]_{fs} - [CO_3^{2-}]_{eq} \right) \qquad (2b)$$

where $[Ca^{2+}]_{sol}$ is the Ca ion concentration in the bulk solution, and it can be assumed that $[Ca^{2+}]_{sol} = [Ca^{2+}]_{fs} \approx [Ca^{2+}]_{eq}$ to a sufficiently good approximation. The concentration of dissolved Ca^{2+} (= 10.4 mmol/L) in the oceans varies little. In general it is not possible to measure $[CO_3^{2-}]_{fs}$, which could potentially be somewhat smaller than $[CO_3^{2-}]_{sol}$, but when calcite growth is occurring under conditions where diffusive transport of $[CO_3^{2-}]$ to the mineral surface is not limiting the growth rate, it is possible to substitute $[CO_3^{2-}]_{sol}$ for $[CO_3^{2-}]_{fs}$ with little loss of accuracy. The equation can then be cast in the following form:

$$R_p = k'_f K_{sp} (\Omega_c - 1) = k_f^* (\Omega_c - 1) \qquad (3a)$$

where Ω_c is the saturation state of the solution with respect to calcite and $K_{sp} = [Ca^{2+}]_{eq}[CO_3^{2-}]_{eq}$, and k_f^* is defined as equal to $k_f K_{sp}$. It has been found experimentally that precipitation rates are not proportional to $(\Omega_c - 1)$, but rather vary as this quantity to a power of up to or even greater then 3 (e.g. Zuddas and Mucci, 1994, 1998; Lopez et al., 2009). It is likely that this higher order dependence stems from changes in the reaction

mechanism with saturation state (e.g. Teng et al., 2000; DeYoreo et al., 2009) and hence equation 3a might better be written:

$$R_p = k_f K_{sp}(\Omega_c - 1) = k_f^*(\Omega_c)(\Omega_c - 1) \quad (3b)$$

where the notation is meant to show k_f^* as a function of Ω_c. Since k_f^* constitutes an estimate for the gross exchange flux at the mineral surface, this point is important in evaluating the isotope fractionation model and its application to trace element partitioning described below. It is also noteworthy that recent studies have shown that k_f^* is dependent on the Ca^{2+}/CO_3^{2-} ratio of the solution (Nehrke et al., 2007; Larsen et al., 2010), which is important for evaluating how the exchange flux R_b relates to k_f^*.

2. MODEL FOR ISOTOPIC FRACTIONATION WITH SURFACE REACTION CONTROL

It is expected that isotopic species such $^{44}Ca^{2+}$ and $^{40}Ca^{2+}$, as well as $^{13}CO_3^{2-}$ and $^{12}CO_3^{2-}$ will have slightly different k_f and k_b values and hence different rates of reaction. The behavior of the C and O isotopes in the carbonate anions is complicated by exchange among dissolved species (e.g. Zeebe and Wolf-Gladrow, 2001), so the analysis here will be restricted to the simpler case of the isotopes of Ca^{2+}. The simplified equations for the rate of attachment (precipitation) of the two Ca isotopic species as mineral crystal growth proceeds can be written:

$$^{40}R_f = {}^{40}k_f[^{40}Ca^{2+}]_{fs}[CO_3^{2-}]_{fs} \quad (4a)$$

$$^{44}R_f = {}^{44}k_f[^{44}Ca^{2+}]_{fs}[CO_3^{2-}]_{fs} \quad (4b)$$

The dissolution rates are:

$$^{40}R_b = {}^{40}k_b[^{40}CaCO_3] \quad (5a)$$

$$^{44}R_b = {}^{44}k_b[{}^{44}CaCO_3] \quad (5b)$$

Implicit in these expressions are the two kinetic isotopic fractionation factors associated with precipitation and dissolution:

$$\alpha_f = \frac{{}^{44}k_f}{{}^{40}k_f} \quad (6a)$$

$$\alpha_b = \frac{{}^{44}k_b}{{}^{40}k_b} \quad (6b)$$

The equilibrium isotopic fractionation factor is:

$$\alpha_{eq} = \frac{\alpha_f}{\alpha_b} = \frac{{}^{44}K_{eq}}{{}^{40}K_{eq}} = \left(\frac{r_{solid}}{r_{fs}}\right)_{eq} \quad (7)$$

where r is shorthand for the isotopic ratio $^{44}Ca/^{40}Ca$. If the above expressions are substituted into the previous equations, two equations can be derived that relate the isotope-specific forward and backward rates (Figure 3):

$$^{44}R_f = \alpha_f \, {}^{40}k_f r_{fs}[{}^{40}Ca^{2+}]_{fs}[CO_3^{2-}]_{fs} = \alpha_f r_{fs} \, {}^{40}R_f \quad (8)$$

and

$$^{44}R_b = \alpha_b \, {}^{40}k_b r_{solid}[{}^{40}CaCO_3] = \alpha_b r_{solid} \, {}^{40}R_b = \frac{\alpha_f}{\alpha_{eq}} r_{solid} \, {}^{40}R_b \quad (9)$$

These equations can be used to derive a general equation for the fractionation attending mineral precipitation under steady state, surface reaction controlled conditions. It should be noted that if the precipitation and dissolution fluxes are equal, the equilibrium condition is recovered. Also, the isotopic effects are not dependent on the exact form of the kinetic rate expression (e.g. equations 2); they are only dependent on the rates themselves.

The effective isotopic fractionation factor for steady state precipitation can be derived starting first with the rate of change of the isotopic ratio of the solid surface layer:

$$r_{solid} = \frac{N_{44Ca}}{N_{40Ca}}$$

where N designates number of atoms (or moles of atoms), and at steady state:

$$\frac{dr_{solid}}{dt} = 0 = \frac{1}{N_{40Ca}}\left(\frac{dN_{44Ca}}{dt} - r_{solid}\frac{dN_{40Ca}}{dt}\right) = \frac{1}{N_{40Ca}}\left({}^{44}R_p - r_{solid}\,{}^{40}R_p\right) \quad (10)$$

Steady state in this case means that the isotopic composition of the surficial layer of the solid is not changing with time as the crystal grows. After substitution of equation 8 and 9 into 10 and some algebraic manipulation, the following expression is obtained for the steady condition (r_{solid} = constant):

$$\alpha_p = \left(\frac{r_{solid}}{r_{fluid}}\right)_{ss} = \frac{\alpha_f}{1 + \frac{R_b}{R_f}\left(\frac{\alpha_f}{\alpha_{eq}} - 1\right)} = \frac{\alpha_f}{1 + \frac{R_b}{R_p + R_b}\left(\frac{\alpha_f}{\alpha_{eq}} - 1\right)} \quad (11)$$

This function is plotted in Figure 4 for arbitrary values of α_{eq} and α_f. The equation describes the instantaneous isotopic fractionation of the material being added to a growing solid phase under conditions where there is no transport limitation. The crossover from equilibrium ($\alpha_p = \alpha_{eq}$) to kinetically controlled ($\alpha_p = \alpha_f$) precipitation occurs at $R_p \approx R_b$. The equation does not take account of any transport in the solid phase that might affect the isotopic composition of the solid surface layer (e.g. Watson, 2004), which at low temperature (ca. 25°C) should be far too slow to affect the process. Transport effects are considered in a later section of the paper.

According to equation 11 and as shown in Figure 4, a critical parameter in assessing isotopic fractionation is the backward (dissolution) rate, R_b, or equivalently the difference between the gross forward precipitation rate R_f and the net forward precipitation rate R_p. For conditions under which $R_p >> R_b$ (or $R_f \approx R_p$) the effective fractionation is dominated by the kinetic fractionation factor associated with precipitation (α_f). In this limit, as shown in Figure 4, the fractionation factor α_p is not sensitive to precipitation rate unless the rate becomes high enough that fluid phase transport limitations start to have an effect. In the other extreme, $R_p << R_b$ (or R_f

$>>R_p$) the equilibrium fractionation is approached. The effective fractionation factor (α_p) is sensitive to precipitation rate mainly in the range where $R_p \approx R_b \approx 2R_f$. The behavior illustrated in Figure 4 and described in equation 11 is what should be expected in the absence of transport effects in the fluid or the solid, and assuming that R_b is not a function of R_p. Comparing with Figure 1, this behavior corresponds to that expected for the conditions represented by the uppermost part of the diagram. It should be noted that R_b, and the values of the kinetic and equilibrium fractionation factors, can be functions of temperature, solution composition, and other variables, but it is inescapable that the approach to equilibrium must depend on the ratio R_p/R_b (or alternatively R_p/R_f).

3. WHAT IS THE VALUE OF R_b?

To apply equation 11 to Ca isotopes in calcite requires values for three parameters – R_b (or R_f), α_f, and α_{eq}. Several studies have reported dissolution rates (i.e. R_b) for calcite. A relatively complete study covering a range of pH values at 25°C was presented by Chou et al. (1989); their data are reproduced in Figure 5. Chou et al. (1989) determined that there is in general more than one dissolution mechanism operating, and the dominant mechanism changes with pH (cf. Alkatten et al., 2009). The available experimental data on Ca isotopic fractionation were obtained using solutions with a relatively narrow pH range of 7.5 to 9 (LeMarchand et al., 2004; Tang et al., 2008), and in this range the value for R_b is invariant with pH and equal to 6 x 10^{-7} mol/m^2/sec at 25°C. For the value of α_{eq}, Fantle and DePaolo (2007) have suggested the value α_{eq} = 1.0000. For α_f, it could be argued based on available data that the value is approximately 0.9985±3, which is the largest fractionation so far observed. However, it is possible that both α_{eq} and α_f vary with temperature, and possibly also with solution composition. The experimental data can also be used to deduce values for α_{eq} and α_f using the proposed model.

The dissolution rate studies in the literature are virtually all done under conditions far from equilibrium; i.e. $\Omega_c << 1$. In this, case, by reference to equation 3b, the value of R_b should be equivalent to the precipitation rate constant:

$$R_b = k_f K_{sp}(\Omega_c - 1) = -k_f K_{sp} = -k_f^* \qquad (12a)$$

As noted above, however the value of k_f* is generally found to be a function of Ω_c, which means that the exchange rate between the mineral surface and the solution is not a constant, but instead tends to vary systematically with oversaturation, especially as (Ω_c - 1) approaches zero. It is even more problematical that k_f* is a function of Ca^{2+}/CO_3^{2-} in the solution (Nehrke et al., 2007; Larsen et al., 2010) because, whereas calcite can precipitate from solutions of arbitrary Ca^{2+}/CO_3^{2-}, it can dissolve only stoichiometrically. Hence the dissolution rate constant k_b (or R_b) is not likely to be equivalent to the precipitation rate

constant k_f^* except when Ca^{2+}/CO_3^{2-}= 1. Nehrke et al (2007) show that k_f^* is roughly 10 times smaller for a seawater-like Ca^{2+}/CO_3^{2-} (≈ 200) than for Ca^{2+}/CO_3^{2-}= 1.

As shown by Teng et al. (2000), the mechanism of calcite mineral growth varies as a function of saturation index, and hence as a function of growth rate. The velocity and spacing of steps, and the density of kinks on the crystal surface determine the growth rate. As oversaturation increases, the spacing of the steps decreases and the step velocities increase, resulting in faster growth rates. Since most of the attachment of ions from solution happens at steps and kinks, the rate of exchange between the mineral surface and the solution is presumably a function of the concentration of steps and kinks, which is also a function of growth rate. The observed growth rate effectively varies as $(\Omega\text{-}1)^n$, where n > 1. A similar conclusion has been reached in other studies although without the benefit of a mechanistic model (e.g. Zuddas and Mucci, 1994; Lopez et al., 2009).

No researcher has proposed a formula relating k_f^* to Ω_c based on the detailed topography and structural evolution of calcite surfaces (cf. DeYoreo, et al., 2009). However, a first-order estimate for the variation of the exchange flux with oversaturation can be inferred from available experimental data on calcite growth rates. If it is assumed that the precipitation rate can be expressed by the following equation:

$$R_p = k_f^*(\Omega)(\Omega_c - 1) \qquad (12b)$$

the exchange flux might vary much like the rate constant $k_f^*(\Omega_c)$, corrected for the solution Ca^{2+}/CO_3^{2-}. Apparent values of k_f^* are derivable from the values of R_p and Ω_c measured in the experiments: $k_f^*(\Omega) = R_p/(\Omega\text{-}1)$. A plot of this apparent exchange rate versus R_p is shown as Figure 6, using data from Tang et al. (2008) and Lopez et al. (2009) acquired at three different temperatures. The data suggest that the apparent rate constant varies roughly as $R_p^{0.5\pm0.2}$ at constant temperature (Figure 6) and for values of R_p between 10^{-9} and 5×10^{-6} mol/m^2/sec. It may be noteworthy that in the experiments summarized in Figure 6, in no case is the 25°C value of k_f^* greater than the value of k_b determined by Chou et al.

(1989). In all cases, the deduced value of k_f* is substantially smaller than k_b. In the discussion below, two versions of the model are used; one with R_b = constant (Model 1), and one in which R_b is allowed to vary with R_p (Model 2) as shown in Figure 6.

3. APPLICATION TO CALCITE PRECIPITATION

3.1 Ca isotopic fractionation in precipitated inorganic calcite

The constant-R_b version of the model applied to Ca isotope fractionation in calcite is shown as Figure 7a. For this calculation, a constant value of R_b = 6 x 10^{-7} mol/m^2/sec at 25°C is assumed, and the resulting model curve is juxtaposed with 25°C data of Tang et al (2008). The dark dashed line in the figure corresponds to limiting fractionation factors of α_{eq} = 0.9995 and α_f = 0.9984. The data fit the model well, which is noteworthy because the inflection point for the curve is set by the value of R_b from Chou et al. (1989) and is not an adjustable parameter. The value of α_f of 0.9984 that fits the data best is consistent with available experimental data. However, the value of α_{eq} that must be used to get a good fit to the data is not that suggested by Fantle and DePaolo (2007), but rather a lower value. The data do not appear to allow for a value of α_{eq} = 1.0000 for the constant-R_b model, as shown by the significantly poorer fit obtained when the model curve is forced to this value. The good fit of the Tang et al (2008) data suggests that the value of R_b derived from the dissolution rate data of Chou et al. (1989) is in fact close to the actual gross molecular exchange flux for Ca between the growing calcite and solution at 25°C, at least in the range of R_p where it is close to the calcite dissolution rate measured by Chou et al. (1989).

A second version of the model is plotted in Figure 7b, where in this case R_b is allowed to vary with R_p. The exact form of the variation of R_b with R_p (or with Ω_c) is not known, although the isotopic data could provide constraints. To evaluate the effect of allowing R_b to vary along the lines of the observations in Figure 6, Model 2 uses an R_b equal to the Chou value at $R_p \geq R_b$, and lets R_b vary as $R_p^{1/2}$ at R_p values lower than the Chou et al. value. The use of values of R_b that are greater than the deduced k_f* values is consistent with the

observations of Nehrke et al. (2007) and Larsen et al. (2010) as noted above, and is required by the fit of the data shown in Figure 7a.

The use of a variable R_b value at low precipitation rates provides a fit to the Ca isotopic data that is similar in quality to that obtained with the constant – R_b model, but it allows the value of α_{eq} to be closer to 1.000; in this case a good fit is obtained with α_{eq} = 0.9998. The other endmember value, is slightly different as well (α_f = 0.9983), but not significantly different from that deduced for the constant-R_b model.

3.2. Effect of temperature on Ca isotopic fractionation

At higher and lower temperature, the value of R_b changes relative to that at 25°C, which shifts the model curve shown in Figure 7 (i.e. α_p versus R_p) toward lower R_p values at lower temperature and higher R_p values at higher temperature. Tang et al. (2008) report data for Ca isotope fractionation at 5°C and 40°C, so the model can be tested against these data. The temperature dependence of the dissolution rate has been determined recently by Gledhill and Morse (2006), albeit in salt-rich brines, and by Pokrovsky et al. (2009). Both studies were done in solutions with lower pH. Here the T-dependence proposed by Pokrovsky et al (2009) is used; which implies that R_b is 1.55 x 10^{-6} mol/m^2/sec at 40°C and 1.5 x 10^{-7} mol/m^2/sec at 5°C, when applied to the 25°C data of Chou et al. (1989) for solutions with pH in range 7.5 to 9. Figures 8a and 8b show the constant-R_b model fits to the Tang et al. (2008) data for 5°C and 40°C. It is evident that the shift in the R_b values due to temperature does well in accounting for most of the data. The model curves were calculated for the same values of α_f and α_{eq} as used for the 25°C model curve.

The curves from Figures 7 and 8 can be used to make inferences about the temperature dependence of the Ca isotope fractionation factor in nature (Figure 9). For example, if R_p is constant and close to the value of 6 x 10^{-7} mol/m^2/sec, there will be a T-dependence to the fractionation factor, with α_p tending toward unity as T increases. This feature is similar to the expectation for equilibrium fractionation, and hence could be confused with the temperature dependence of an equilibrium fractionation factor (e.g. Gussone et al., 2003).

However, the kinetically controlled T-dependence will depend in turn on the precipitation rate. Figure 8 shows the expected T-dependence of α_p, for five different values of R_p. At R_p = 6 x 10^{-7} mol/m^2/sec, there is the maximum T-dependence, and over the range of temperature appropriate to the oceans (0 to 40°C), the value of 1000lnα_p shifts by about 0.6‰. However, at higher and lower values of R_p, there is less T-dependence.

For biogenic calcite formation, organisms may produce calcite from solutions that are oversaturated by a factor of 5 to 10 (slightly in excess of that of surface seawater; e.g. Bentov and Erez, 2005), hence the attendant R_p values may be close to 10^{-6} mol/m^2/sec or somewhat lower due to the inhibiting effect of Mg ions. At this rate one would expect approximately the observed variation of about 0.5‰ as shown on Figure 9. Since aragonite dissolves at about the same rate as calcite (i.e. R_b for aragonite is the same as that for calcite; Chou et al., 1989), the temperature variability for aragonite is likely to be similar to that for calcite at the same precipitation rate, as is indicated by the data of Gussone et al (2003), although the fractionation factor is somewhat larger. The data and model curves shown in Figure 9 suggest that the temperature dependence of R_b could play a significant role in determining isotopic fractionation in biogenic as well as abiogenic calcite. However, it is well known that many organisms produce microenvironments from which calcite is precipitated, and therefore other effects could also contribute to the observed fractionations (e.g. Bentov and Erez, 2005; Sime et al, 2005; Carre et al., 2006).

3.3. Trace element incorporation into calcite

The incorporation of trace metal cations (e.g. Sr, Ba, Mn, Cd, U) into calcite is analogous in many ways to isotopic fractionation and hence may also be treatable with an appropriate modification of equation 11. One difference between trace element-to-Ca ratios and Ca isotope ratios, is that the former vary over a factor of 10 or more with varying precipitation rate rather than over just a few tenths of a percent. As shown here, this difference may be important for constraining the precipitation rate-dependence of the molecular exchange rates at the mineral surface.

For illustration, the Sr/Ca ratio of calcite is used, where there are data from several sources relating Sr/Ca to precipitation rate (Tang et al., 2008; Tesoriero and Pankow, 1996; Lorens, 1981; Gabitov and Watson, 2006). The model can be applied to the Sr/Ca elemental ratio in a straightforward manner if it is assumed that the range of Sr concentrations is well within the Henry's law regime for the solid; i.e. that the activity coefficient for Sr in calcite is a constant. Making this assumption, the above equations for isotopes need only be modified by substituting Sr for ^{44}Ca, and Ca for ^{40}Ca, and α is replaced with "K" as defined below.

$$K_{p,Sr} = \left(\frac{(Sr/Ca)_{solid}}{(Sr/Ca)_{fluid}} \right)_{ss} = \frac{K_f}{1 + \frac{R_b}{R_p + R_b}\left(\frac{K_f}{K_{eq}} - 1\right)} \tag{13}$$

where $K_f = k_{f,Sr}/k_{f,Ca}$ is the forward kinetic fractionation factor for Sr/Ca in the precipitation reaction, and K_{eq} is the equilibrium Sr/Ca partition coefficient applicable to extremely slow precipitation and determined by the activity coefficient of $SrCO_3$ dissolved in calcite. As with Ca isotope fractionation, $K_{p,Sr}$ has been determined experimentally to be dependent on precipitation rate. At low precipitation rates (≤ 10^{-8} mol/m^2/sec) the value is ostensibly between about 0.02 and 0.07, and at high precipitation rates it is in the range 0.24 to 0.4 (Gabitov and Watson, 2006).

Figure 10 shows plots of equation 13, with constant R_b, juxtaposed against 25°C experimental data from Tang et al. (2008), Tesoriero and Pankow (1996), and Lorens (1981). In each case, the input parameters are the calcite dissolution rate from Chou et al. (1989) (adjusted for temperature and at the appropriate pH), K_{eq}, and K_f. In all cases, a value of $K_f = 0.24$ is used. For the Tang et al. (2007) data, K_{eq} is set equal to 0.07, whereas for the Tesoriero and Pankow (1996) data K_{eq} is set equal to 0.03, and for Lorens (1981) K_{eq} is set equal to 0.035. The data for the Tesoriero and Pankow (1996) study were obtained at pH ≈ 6.2, substantially lower than the pH ≈ 8 used in the Tang et al. (2008) study and the pH ≈ 7.4 used by Lorens (1981). Tang et al. (2008) give reasons why K_{eq} could be pH-dependent, but in any case, to fit the data the only parameter that needs to be

adjusted between the three studies is K_{eq}, and this adjustment is unavoidable because the three studies obtained different values of $K_{p,Sr}$ at similar R_p values of about 10^{-7} mol/m^2/sec. The lower pH of the Tesoriero and Pankow (1996) study also necessitates the use of a slightly higher value of R_b at 25°C of 1 x 10^{-6} mol/m^2/sec (see Figure 5). All of the Sr/Ca partitioning data are well described by the constant-R_b model, given the adjustment of K_{eq} with pH. The Lorens (1981) data could be fit better if a lower value of K_f were used, but there is also some uncertainty about their precipitation rates, since they did not carefully control the reacting surface area. The model fits the data of Gabitov and Watson (2006) also; they found a relatively large range of K_p values at very high precipitation rates, but the value of K_f = 0.24 fits with the lower range of their values. The one worrisome aspect of the data shown in Figure 10 is the difference between the Tang et al. (2008) results and those of Lorens (1981) and Tesoriero and Pankow (1996). The results from the latter two studies are similar, especially if corrected for pH. The Tang et al (2008) Sr/Ca data appear to be shifted to lower R_p values, which could mean that they have slightly underestimated the precipitation rates for their experiments. If they have, it would require some revision to the interpretations of the Ca isotope data given above.

Given the good fit of the Sr/Ca data it follows that the model could also be applicable to U, Cd, Ba, Mn, and other trace elements in calcite. The data for Mn/Ca partitioning from Lorens (1981) are among the best available for testing the model and are interesting because the apparent equilibrium Mn/Ca ratio (i.e. the value at low R_p values) is much larger than the kinetically-controlled Mn/Ca, and both values are far from unity. Figure 11 shows the Lorens (1981) Sr/Ca data compared to a fit using the variable – R_b model (Model 2), and also shows the Lorens (1981) Mn/Ca data with curves representing both the constant – R_b (Model 1) and the variable-R_b (Model 2) versions of the model. The Model 2 fit to the Lorens Sr/Ca data is marginally better than the Model 1 fit shown in Figure 10. For the Lorens Mn/Ca data, however, the two models differ substantially, and only Model 2 appears to fit the entire data set reasonably well. This result could be regarded as evidence that the molecular exchange rate does indeed vary substantially at low Ω_c and R_p values.

3.4. Oxygen isotopes in precipitated calcite

Kinetic effects on oxygen isotope fractionation during calcite precipitation are of broad interest for paleo-environmental studies. Dietzel et al (2009) present data showing that the fractionation of $^{18}O/^{16}O$ between calcite and solution grown in the laboratory at constant temperature and pH is dependent on precipitation rate. Analysis of this effect is more complicated than that for Ca isotopes. Traditionally, most workers have discussed O isotope fractionation in terms of the difference between calcite and water. This difference is large – close to +30‰ at 25°C. Zeebe (1999) and Zeebe and Gladrow (2001), on the other hand, propose that the important fractionation factors are between calcite and the dissolved carbonate species (mostly HCO_3^- and CO_3^{2-}) in solution in the water. Zeebe (1999) has noted that the equilibrium fractionation between calcite and the average carbonate species in solution is close to zero (i.e. $\alpha_{eq} = 1.0000$ relative to bulk DIC) and that calcite tends to inherit the average isotopic composition of the dissolved inorganic carbon (DIC).

For our purposes, comparing the $\delta^{18}O$ of calcite CO_3 to that of total DIC is analogous to comparing the $\delta^{44}Ca$ of calcite with that of dissolved Ca^{2+}. Dietzel et al give the $\delta^{18}O$ values of their precipitated calcite relative to $\delta^{18}O$ of the water from which the calcite was precipitated. From the calcite - water fractionation values and inter-species fractionation factors given by Beck et al. (2005) it is possible to calculate the $\delta^{18}O$ of the carbonate species in solution, and from those and the pH the $\delta^{18}O$ of the bulk DIC. A plot of $\delta^{18}O$ of precipitated calcite relative to bulk DIC (at 25°C; from Dietzel et al., 2009) versus precipitation rate is shown as Figure 12. The data follow the predicted trends reasonably well for either the constant-R_b or variable-R_b models. This result suggests that the fractionation of O isotopes may not be so different from that of Ca in that the equilibrium fractionation between the solid phase and dissolved species is small, and much of the observed variation may be due to kinetic effects during non-equilibrium precipitation of $CaCO_3$. This result does not mean that carbonate $\delta^{18}O$ does not reflect temperature, just that the temperature effects are associated with isotopic exchange between the dissolved carbonate species and water.

4. DISCUSSION AND IMPLICATIONS

4.1 Isotopic effects due to transport limitations in the fluid phase

The agreement of the Tang et al (2008) Ca isotope results and the model curves shown above would not be expected if the Tang et al. precipitations occurred under conditions where the delivery of Ca^{2+} ions to the mineral surfaces was transport - controlled. There are strong arguments why the Tang et al. experiments must have been in the surface reaction control regime. The experimental conditions were such that $[Ca^{2+}] >> [CO_3^{2-}]$, so the surface reaction control limit to the precipitation rate is determined by the delivery of carbonate ions to the mineral surface, not the delivery of Ca ions. Also, the Tang et al. precipitation rates as a function of oversaturation are very close to those of Lopez et al. (2009), who employed a fluidized bed arrangement, which should guarantee surface reaction control at pH > 7. Hence it is highly likely that the Tang et al (2008) data represent a surface reaction-controlled condition for Ca isotope fractionation.

To evaluate other experiments, and the limits of the surface reaction model, it is useful to derive an approximate formulation for the effects of transport. If the advance of a growing calcite crystal face is limited by diffusion of CO_3^{2-} through a boundary layer of thickness h_{bl} (Figure 13), the following equation must be satisfied:

$$D_{CO_3}\frac{[CO_3^{2-}]_{sol}-[CO_3^{2-}]_{fs}}{h_{bl}} = k_f[Ca^{2+}]_{sol}\left([CO_3^{2-}]_{fs}-[CO_3^{2-}]_{eq}\right) \qquad (13a)$$

This equation results from equating the rate of diffusion of CO_3^{2-} ions through the boundary layer (left side) to the deposition rate on the surface of the crystal (from equation 2b). This formulation is valid because the rate of crystal growth is small enough that the condition $vh_{bl}/D_{CO_3} << 1$ is satisfied, where v is the growth velocity of the crystal. Rearranging equation 13a, we can write:

$$\frac{D_{CO_3}}{h_{bl}k_f[Ca^{2+}]_{sol}} = \frac{[CO_3^{2-}]_{fs} - [CO_3^{2-}]_{eq}}{[CO_3^{2-}]_{sol} - [CO_3^{2-}]_{fs}} \quad (13b)$$

The conditions under which the right side of this equation is equal to unity can be defined as the point where diffusion and surface reaction are of equal importance. The critical boundary layer thickness at which this transition point occurs is:

$$h^*_{CO_3} = \frac{D_{CO_3}}{k_f[Ca^{2+}]_{sol}} = \frac{D_{CO_3}[CO_3^{2-}]_{eq}}{k^*_f} \quad (14)$$

where the subscript CO_3 is meant to imply the critical boundary layer thickness under the condition that $[Ca^{2+}] > [CO_3^{2-}]$.

Using the values D_{CO3} = 8 x 10^{-10} m^2/sec, k_f^*= 6 x 10^{-8} mol/m^2/sec (a mid-range experimental value, from Figure 6), and $[CO_3^{2-}]$ = 0 .043 mol/m^3 (corresponding to equilibrium with seawater; Ca^{2+} = 10 mol/m^3), results in h^*_{CO3} = 0.6 mm. If stirring a beaker at 150 to 300 rpm produces diffusional boundary layers that are similar to those of a rotating disk at the same rates (e.g. Alkatten et al., 2007), then the diffusive boundary layer thicknesses would be in the range 15-25 μm, well below the critical boundary layer thickness. Consequently, stirred experiments at high pH should be in the surface reaction controlled regime. However, the rate of calcite precipitation in an unstirred precipitation experiment could be affected by transport because boundary layer thicknesses are likely to be much larger. However, for a solution where $[Ca^{2+}] >> [CO_3^{2-}]$ it is less likely for Ca supply to be transport controlled because, if the rate of delivery of Ca^{2+} by diffusion is to be equal to the rate of delivery of CO_3^{2-}, the drawdown in $[Ca^{2+}]$ near the crystal surface cannot be greater than $[CO_3^{2-}]$, which is small relative to $[Ca^{2+}]$.

It should be noted that equation 14 indicates that the critical boundary layer thickness is dependent on $[Ca^{2+}]$. At lower $[Ca^{2+}]$, for example if it is equal to $[CO_3^{2-}]$ so that both are 0.66 mol/m^3, the critical boundary layer thickness increases to $h^*_{CO3} \approx 9$ mm. Hence it may be easier to achieve conditions of surface reaction controlled precipitation if the solution

has $[Ca^{2+}] = [CO_3^{2-}]$, although this effect could be offset by changes in k_f^* as a function of Ca^{2+}/CO_3^{2-}. In the other extreme, for a solution with very high $[Ca^{2+}]$, for example, 150 mol/m^3 (Lemarchand et al., 2004), the calculated critical boundary layer thickness decreases to 40 μm, which creates conditions where it may be more difficult to avoid transport limitations on the precipitation rate even in stirred solutions.

Experimental results of Richter et al. (2006) indicate that the ratio of the diffusivities of $^{44}Ca^{2+}$ and $^{40}Ca^{2+}$ in chloride solution is approximately 0.9945. Assuming that this value applies to the experimental solutions of Tang et al. (2008), if calcite growth were controlled by transport of Ca^{2+} ions to the crystal surface, we would expect a fractionation of $\Delta^{44}Ca$ = -0.55 permil (α_{diff} = 0.9945). The larger fractionations observed suggest that transport effects do not dominate the results.

4.2 Experiments of Lemarchand et al (2004)

Lemarchand et al (2004) report Ca isotope fractionation factors for calcite precipitated from $CaCl_2$ –NH_4Cl solutions. They also found a relationship between calcite precipitation rate and Ca isotope fractionation, although the relationship is opposite to that of the Tang et al (2008) results even though the estimated range of precipitation rates is similar. At high precipitation rates Lemarchand et al (2004) found small fractionations approaching $\Delta^{44}Ca$ = 0, and at slower precipitation rates they found larger fractionations approaching $\Delta^{44}Ca$ = -1.3. In most of their experiments, they diffused CO_2 into the solutions from the top and did not stir the solutions. As they describe, their solutions were heterogeneous, with high $[CO_3^{2-}]$ at the liquid surface and strong diffusive gradients downward into the solution. With no stirring, the precipitation rates may have been transport – controlled. Lemarchand et al did not measure the precipitation rates, but rather calculated them from an equation given by Zuddas and Mucci (1994), which gives a relationship between precipitation rate and solution oversaturation. However, the equation given by the latter authors was determined for surface reaction-controlled conditions using a fluidized bed experimental arrangement. It is unclear whether the reported, calculated precipitation rates of Lemarchand et al are accurate. Also, because of the geometry of the experiments, it is likely

that the rates were variable, both in space and time. As crystallization occurred along the sides of the shallow (3 cm deep, 8 cm diameter) beaker, CO_3^{2-} ions could have been delivered from the top surface while Ca^{2+} ions need to diffuse laterally. In this geometry it is possible that Ca^{2+} gradients could have been large enough to produce isotopic effects due to diffusive transport. However, because they observed fractionations that are smaller than -0.55 permil, the fractionation must not have been controlled by a steady state process such as that depicted in Figure 13, but either to depletion of aqueous Ca in a boundary layer near the growing calcite crystals or a different mechanism of precipitation that is accessed only at very high solution oversaturation.

To evaluate whether aqueous Ca depletion is likely in the Lemarchand et al. experiments, consider a hypothetical situation where the precipitation rate is controlled independent of solution chemistry. The thickness of a boundary layer where depletion of Ca by precipitation onto a growing crystal is balanced by diffusion into the layer is:

$$h_{Ca} = \frac{D_{Ca}[Ca^{2+}]}{R_p} \qquad (15)$$

In the Lemarchand et al unstirred experiments with the highest precipitation rates (estimated at 10^{-5} mol/m^2/sec), and for $[Ca^{2+}]_{sol}$ = 15 - 150 mol/m^3 , the value of h_{Ca} is about 1.2 mm to 12 mm. In unstirred conditions, this could be in a regime where Ca transport is limiting since these estimated h_{Ca} values are smaller than the 40 mm radius of the beaker. The actual precipitation rates could locally have been higher or lower than the authors' estimates. In general, however, as the precipitation rate is lowered toward 10^{-7} mol/m^2/sec, transport should be less important and the surface reaction control limit should be approached, which could explain the relationship Lemarchand et al. observed between precipitation rate and Ca isotope fractionation. However, it is still not possible to reconcile the results of the two studies unless the precipitation rate estimates in one or both studies are in error by a large factor (cf. Tang et al., 2008). In addition, Gussone et al. (2005) found a relationship between Ca isotope fractionation and precipitation rate in aragonite that is similar to that determined by Lemarchand et al. for calcite.

4.4. Previously proposed growth entrapment models

An alternative model for the control on trace element incorporation into calcite has been advanced by Watson (2004), who describes a "growth entrapment model," whereby the precipitation rate dependence of Sr/Ca (and other ratios involving trace constituents) in calcite arises from a competition between mineral growth rate, expressed in terms of a growth velocity (v) normal to the crystal surface, and the redistribution of the trace constituent back to the mineral surface by solid state diffusion. The growth velocity is proportional to the precipitation rate used here according to: $v = R_p M_s/\rho_s$, where M_s is the molecular weight of the solid and ρ_s the density. In the Watson (2004) model the competition is expressed as a Peclet number that compares the timescale to accumulate a thickness L of new mineral material (L/v), with the timescale required for diffusion within this layer (L^2/D) to allow expulsion of excess Sr back to the surface. The value of L needs to be in the range of a few molecular dimensions (or ca. 10^{-9} m) for the model to apply, because it is the thermodynamic properties of these near surface layers that drive the inferred diffusion, and Fenter et al (2004) for example, have shown that only the outermost one or two molecular layers of calcite are different from the bulk in terms of bond lengths and orientation.

For a typical growth rate of 10^{-6} mol/m^2/sec, the growth velocity is $v = 3.7 \times 10^{-11}$ m/sec. In order for Sr diffusion in the solid to compete with growth, the diffusivity needs to be about 10^{-20} m^2/sec. The expected value of the volume diffusivity of Sr in calcite at 25 °C (extrapolated from higher temperature data) is 1.5×10^{-36} m^2/sec (Cherniak, 1997), about 10^{16} times smaller. This result would seem to indicate that diffusion within the crystal is not significant, and the explanation for the growth rate dependence must lie elsewhere. Recognizing the disparity, Watson (2004) postulates that there is an effective diffusivity of just the right order of magnitude (ca. 10^{-15} to 10^{-20} m^2/sec) that applies only over a distance of about one atomic layer at the crystal surface, and that the diffusivity decreases systematically over a distance of one or two molecular layers into the crystal. He suggests

that this is not really diffusion but ionic mobility or exchange between near-surface layers. Nevertheless, the process is formulated as diffusion in the model.

A key postulate of the Watson (2004) model, taken from the original model for sector zoning in igneous minerals (Watson and Liang, 1995; Watson, 1996), is that the surface layer of the calcite crystal is maintained in equilibrium with the solution during growth. The model posits that the surface layer, of one or two molecular dimensions thickness (ca. 0.5 nm), has a different crystal structure and hence different *equilibrium* concentration of trace elements and isotopes. It is the difference in the equilibrium chemical potential (or activity coefficient) between the crystal interior and the surface layer that drives diffusion and the approach to the new (crystal interior) equilibrium concentration as the crystal grows. As noted above, however, the surface layer is not likely to be in equilibrium with the solution except at very slow crystal growth rates. Most calcite grown in the laboratory (or biogenically) is precipitated under conditions of substantial oversaturation, and there is no reason to expect that equilibrium can be maintained. If the surface layer is not kept at equilibrium with the solution by infinitely fast exchange, then the surface boundary condition for the Watson (2004) model is not correct, and the driving force for uphill diffusion to the surface is undefined.

The Watson (2004) surface entrapment model (SEMO; see also Gaetani and Cohen, 2006; Tang et al., 2008) yields growth rate dependence that is similar to the model presented here, although not identical. The kinetic effects in both models are controlled by a dimensionless number, which relates the growth velocity (v or $R_p M_s/\rho_s$) to a "relaxation velocity" (D_s/L or $R_b M_s/\rho_s$). In applying the SEMO model to their Ca isotope data obtained at different temperatures, Tang et al (2008) show that it is necessary to systematically change the parameter F_{44Ca}, which is analogous to the parameter α_f in the model presented here. Hence the SEMO model requires that this parameter have substantial temperature dependence whereas in the model presented here, the Tang et al. (2008) data can be fit with no change in α_f between 5°C and 40°C. Hence the two models predict substantially different behavior in the high precipitation rate (high R_p) limit. Interestingly, Tang et al.

(2008) were able to fit their data with the SEMO model with a low temperature limit of α_{eq} = 1.000. They also show that temperature dependence similar to that shown in Figure 9 for $\Delta^{44}Ca$ can be obtained from the SEMO model with the appropriate choice of parameters.

The model presented here is also in effect a "growth entrapment model," but the competition is between the growth rate and the rate of molecular exchange between the mineral surface and solution. In comparison to the Watson (2004) model, the model presented here is attractive in that the approximate value of v (or R_p) at which there are strong effects on trace element and isotopic partitioning, is predictable from measureable rates of dissolution or from the experimentally determined kinetic rate constants for the precipitation reaction.

4.5. Ultra-slow reaction rates and surface exchange rates

As noted above, the apparent equilibrium Ca isotope fractionation factor at slow precipitation rates approaching 10^{-8} mol/m^2/sec is 0.9995 (or 1000 ln α_{eq} = -0.5) for the constant- R_b version of the model (Model 1), and 0.9998 for the variable-R_b version of the model (Model 2). Neither value is exactly the value 1.0000 inferred from deep-sea sediment pore fluids from ODP Site 807 by Fantle and DePaolo (2007). The differences are subtle, but probably significant. The discrepancy may relate to the extremely slow inferred rate of precipitation of calcite in the Site 807 pore fluids (see also Richter and Liang, 1993), which are far slower than in the experiments. To illustrate the difference between the pore fluids and the available laboratory experiments, if precipitation in the Site 807 sediments were distributed over the available surface area of the sediment, the rate would be 10^{-17} to 10^{-18} mol/m^2/sec (Fantle and DePaolo, 2007), some 9 to 10 orders of magnitude slower than those accessed by laboratory experiments. If the active surface area of the Site 807 sediments is, for example, 10^4 times smaller than the total surface area, the observed precipitation rate is still 4 to 5 orders of magnitude smaller than those of the laboratory experiments. In the formulations provided here of the Ca exchange rate at the mineral surface, it is shown that if the exchange rate decreases at low Ω_c (and R_p), it is possible to bring the laboratory results for Ca isotopic fractionation closer to agreement with the

results from deep sea pore fluids. The Mn/Ca data of Lorens (1981), and the many studies of calcite precipitation mechanisms, provide evidence that the exchange rate does decrease as equilibrium conditions are approached. Fantle and DePaolo (2007) argue that Ω_c must be indistinguishable from unity in Site 807 pore fluid, so the system is very close to equilibrium. For conditions that are incrementally displaced from equilibrium, and for systems that are allowed to mature for millions of years, we do not know what the surface exchange rates are; they could be even slower than would be inferred by extrapolation of the data in Figure 6. Ultimately, to fully reconcile the laboratory and pore fluid observations, a better measure of (or model for) the molecular exchange rates at the mineral surface is necessary. Additional complications can arise from the effects of the presence of trace constituents, including organic compounds, which may significantly change the rates of molecular exchange (e.g. Morse etal., 1997; Wasylenki et al., 2005a, b; Stephenson et al, 2008). Also, at extremely slow growth rates it is possible that solid state diffusion could play a role, if for example the diffusivity is larger than would be indicated by extrapolation from higher temperature experimental data (e.g. Marshall et al., 1986), and if there is somewhat accelerated atomic exchange between near surface layers as hypothesized by Watson (2004).

4.7. Origins of kinetic fractionation during precipitation

Although there is as yet no definitive information on the origin of kinetic isotopic and trace element fractionations during precipitation, it may be a useful working hypothesis that the kinetic effects are associated with dehydration of dissolved ions during the precipitation step, and rehydration during the dissolution step. In any reaction where a chemical bond must be broken to release the reactant, it is expected that the rate of bond breaking, and hence the rate of reaction, will be higher for the light isotopic species (e.g. Criss, 1999; Zeebe, 2001). Bond breaking involving the light isotopic species is favored because it has a higher zero-point vibrational energy and hence has a slightly smaller potential energy barrier to overcome. The attachment of Ca^{2+} ions to a calcite mineral surface may involve an initial step of formation of an outer sphere complex, in which the Ca^{2+} is still surrounded by a shell of water molecules, followed by formation of an inner sphere complex that

requires dehydration (e.g. Morse et al., 2007). It is likely that the kinetics of dehydration favor the light isotope, and it is possible that this step is the one that results in the forward isotopic fractionation factor α_f, having a value less than unity. For analogous reasons the release of Ca^{2+} from the mineral surface back to solution is also likely to favor the light isotope so that α_b is less than unity. If these two fractionation factors are close in value, then the equilibrium fractionation factor should be close to unity.

If the dehydration/rehydration of Ca^{2+} ions is the major factor controlling the kinetic fractionation factors, then any perturbation to the stability of the hydration shell, such as effects due to other constituents in solution, could alter the kinetic fractionation factors as well as the reaction rates. Relative rates of dehydration might also partly explain the forward kinetic fractionation factors for Sr/Ca partitioning. The relatively larger ionic radius of Sr^{2+} relative to Ca^{2+} presumably makes it easier to dehydrate, and this may be the reason that the forward precipitation reaction favors the incorporation of Sr in calcite in excess of the equilibrium value. As with isotopic partitioning, changes in the strength of ion hydration due to solution chemistry could affect the kinetic fractionation factor for Sr/Ca. However, it cannot be ignored that the presence of impurities like Sr and Mg on the calcite surface also affects the mineral growth rate and mechanism (Wasylenki et al., 2005a, b; Katz, 1973; Davis et al., 2000), and hence there may be complex feedbacks between growth rate, kinetic fractionation factors, and molecular exchange rates between mineral and solution.

5. CONCLUSIONS

The Ca and O isotopic fractionation during precipitation of calcite from aqueous solution provides critical information on the molecular exchange fluxes at the mineral-solution interface during mineral growth. These fluxes are not easily measureable by other methods, but are critical for understanding the dynamics of the interface and for understanding isotopic partitioning. A relatively simple model describing how isotopic fractionation during precipitation should depend on precipitation rate is presented. The key parameters in the model are the forward (precipitation reaction) fractionation factor,

α_f, the equilibrium fractionation factor, α_{eq}, and the bulk backward reaction rate R_b. The latter is effectively the value of the gross exchange flux at the interface. The ratio of the net precipitation rate R_p to the exchange flux R_b determines whether the isotopic fractionation during precipitation is close to the equilibrium value ($R_p/R_b << 1$) or the forward kinetic fractionation factor ($R_p/R_b \geq 1$). A key question is how to estimate R_b. It is posited here that R_b is equal to the dissolution rate of the mineral into a highly undersaturated solution, assuming that there are no transport limitations affecting the dissolution rate. This assumption leads to a first version of the model (Model 1) in which R_b is assumed to be constant, i.e. independent of solution saturation state and precipitation rate. Model 1 achieves excellent fits of available Ca and O isotope data (from Tang et al., 2008; and Dietzel et al., 2009), and for Sr/Ca partitioning for pH of 7 to 9 (from Tang et al., 2008; Tesoriero and Pankow, 1996; Lorens, 1981; and Gabitov and Watson, 2006), which suggests that it has merit.

The far-from equilibrium dissolution rate may be only a starting point for understanding the dynamics of precipitation and their effects on isotopic and trace element partitioning. The primary success shown here is that the transition between near-equilibrium isotopic fractionation and fractionation controlled by the forward kinetic fractionation factor, occurs as predicted at a value of $R_p \approx R_b$, where R_b is the value of the calcite dissolution rate determined by Chou et al (1989) at the appropriate pH and temperature. But, available data suggest that the value of R_b decreases at low solution oversaturation and low net precipitation rates (e.g. Teng et al., 2000; DeYoreo et al., 2009). To account for this effect, a second version of the model (Model 2) is presented where R_b is allowed to vary as $R_p^{1/2}$ at low R_p values. This second version of the model fits the Ca and O isotopic data, and the Sr/Ca partitioning data, no better than the constant-R_b version of the model, but it fits the Mn/Ca data of Lorens (1981) much better. Model 1 does not allow for extrapolation of the laboratory Ca isotope fractionation data to an equilibrium fractionation factor of α_{eq} = 1.0000, as suggested by Fantle and DePaolo (2007) from studies of deep sea pore fluids. Model 2 comes close to allowing the laboratory and pore fluid data to be reconciled. Both models suggest that the Ca isotope fractionation factor for the forward reaction is close to

α_f = 0.9984. Any extension to the model may need to account for potential changes in R_b as a function of solution composition (e.g. presence of Mg, Sr, Na, K, and other anion components and organic solutes).

The model described here derives from standard macroscopic formulations of the kinetic controls on mineral precipitation, and the precipitation rate dependence arises from the inescapable consideration that the net precipitation rate can be either similar to or much smaller than the gross precipitation flux. The model is also anchored on a measureable parameter – the far-from-equilibrium dissolution rate of calcite. The implication of the agreement between model and data is that the major control on both Ca isotope composition and Sr/Ca in calcite is the competition between net and gross precipitation rates.

The model presented here explains the precipitation rate dependence of isotopic and trace element partitioning into calcite by means of a "growth entrapment model," where there is an implicit competition between the mineral-solution exchange rate (represented by the far-from-equilibrium dissolution rate R_b), and the net precipitation rate (R_p). Watson (2004) presents an alternative growth entrapment model to explain the same precipitation rate dependence in terms of a competition between solid-state diffusion within the growing calcite crystal and the net precipitation rate. There is an unsatisfactory aspect of the Watson model in that the measured solid state diffusion rate is many orders of magnitude too small to be competitive with the precipitation rate, and hence it may be that the model presented here is a better description of the mineral surface processes controlling isotopic and trace element partitioning at low temperatures. However, solid-state transport may come into play at sufficiently slow mineral growth rates and at higher temperatures (e.g. Watson and Liang, 1995; Watson, 1996), especially if low-temperature diffusivities are anomalously high and if atomic exchange among a few near –surface molecular layers is significantly faster than bulk diffusion.

6. ACKNOWLEDGEMENTS

This manuscript has benefited from comments and discussion with James Watkins, Carl Steefel, Ian Bourg, Laura Nielsen, James DeYoreo, Patricia Dove, Matt Fantle, Rick Ryerson, and Bruce Watson. Comments by the reviewers, including R.I. Gabitov and the AE Edwin Schauble, were also beneficial. This work was supported by the Director, Office of Science, Office of Basic Energy Sciences, Chemical Sciences Geosciences and Bioscience Program of the U.S. Department of Energy under Contract No. DE-AC02-05CH11231, partly through the Center for Nanoscale Control of Geologic CO_2, an Energy Frontier Research Center.

7. REFERENCES

Alkattan, M., Oelkers, E., Dandurand, J.-L., and Schott, J., 2002, An experimental study of calcite dissolution rates at acidic conditions and 25 °C in the presence of $NaPO_3$ and $MgCl_2$, Chemical Geology, v. 151, p. 199-214.

Bentov, S. and Erez, J. (2005) Novel observations on biomineralization processes in foraminifera and implications for Mg/Ca ratio in the shells. *Geology* **33**(11), 841-844.

Beck, W.C., Grossman, E.L. and Morse, J.W. (2005) Experimental studies of oxygen isotope fractionation in the carbonic acid system at 15°, 25°, and 40°C. *Geochimica et Cosmochimica Acta*, 69, 14, 3493–3503.

Beck, J.W., Edwards, R.L., Ito, E., Taylor, F.W., Récy, J., Rougerie, F., Joannot, P. and Henin, C. (1992) Sea–surface temperature from coral skeletal strontium/calcium ratios, *Science* 257 , 644–647.

Carre´ M., Bentaleb I., Bruguier O., Ordinola E., Barrett N. T. and Fontugne M. (2006) Calcification rate influence on trace element concentrations in aragonitic bivalve shells: evidences and mechanisms. *Geochim. Cosmochim. Acta* 70, 4906–4920.

Cherniak D. J. (1997) An experimental study of strontium and lead diffusion in calcite, and implications for carbonate diagenesis and metamorphism. *Geochim. Cosmochim. Acta* 61, 4173–4179.

Chou, L., Garrels, R.M., and Wollast, R. (1989) Comparative study of the kinetics and mechanisms of dissolution of carbonate minerals. *Chemical Geology*, 78, 269-282

Coggon, R.M., Teagle, D.A.H., Smith-Duque, C.E., Alt, J.C. and Cooper, M.J. (2010) Reconstructing Past Seawater Mg/Ca and Sr/Ca from Mid-Ocean Ridge Flank Calcium Carbonate Veins. *Science* 327, 1114-1117.

Criss, R. E. (1999) *Principles of stable isotope distribution*. Oxford University Press, New York.

Davidovits, P. Worsnop, D., Jayne, J., Kolb, C., Winkler, P., Vrtala, A., Wagner, P., Kulmala, M., Lehtinen, K., Vesala, T., and Mozurkewich, M., 2004, Mass accommodation coefficient of water vapor on liquid water, Geophysical Research Letters, v. 31, L22111.

Davis K. J., Dove P. M., and De Yoreo J. J. (2000) The role of Mg^{2+} as an impurity in calcite growth. *Science* 290, 1134–1137.

De La Rocha, C. L. and DePaolo, D. J. (2000) Isotopic evidence for variations in the marine calcium cycle over the Cenozoic. *Science* **289**(5482), 1176-1178.

DePaolo, D. J. (2004) Calcium isotopic variations produced by biological, kinetic, radiogenic and nucleosynthetic processes. In *Geochemistry of non-traditional stable isotopes*, Vol. 55 (ed. Johnson, C. M., Beard, B. L., and Albarede, F.), pp. 255-285. Mineralogical Society of America; Geochemical Society.

DeYoreo, J.J., Zepeda-Ruiz, L. A., Friddle, R. W., Qiu, S. R., Wasylenki, L.E., Chernov, A. A., Gilmer, G. H. and Dove, P. M. (2009) Rethinking classical crystal growth models through molecular scale insights: Consequences of kink-limited kinetics. *Crystal Growth & Design*, Vol. 9, No. 12, 5135-5144.

Dietzel M., Gussone N. and Eisenhauer A. (2004) Co-precipitation of Sr^{2+} and Ba^{2+} with aragonite by membrane diffusion of CO_2 between 10 and 50°C. *Chem. Geol.* 203, 139–151.

Dietzel, M., Tang, J., Leis, A., and Köhler, S.J. (2009) Oxygen isotopic fractionation during inorganic calcite precipitation — Effects of temperature, precipitation rate and pH. *Chemical Geology* 268, 107–115

Eisenhauer, A., Kisakurek, B., and Bohm, F., 2010, Marine calcification: An alkali earth metal isotope perspective, Elements, v. 5. P. 365-368.

Fantle, M. S. and DePaolo, D. J. (2005) Variations in the marine Ca cycle over the past 20 million years. *Earth Planet Sci Lett* **237**(1-2), 102-117.

Fantle, M.S. and DePaolo, D.J. (2007) Ca isotopes in carbonate sediment and pore fluid from ODP Site 807A: The Ca^{2+}(aq)-calcite equilibrium fractionation factor and calcite recrystallization rates in Pleistocene sediments. *Geochim.* Cos*mochim. Acta,* v. 71, 2524-2546.

Fenter, P., Geissbühler, P., Dimasi, E., Srajer, G., Sorensen, L. B. and Sturchio, N. C., 2000, Surface speciation of calcite observed in situ by high-resolution X-ray reflectivity. *Geochimica et Cosmochimica Acta*, Vol. 64, 1221–1228.

Gabitov, R.I. and Watson, E.B. (2006) Partitioning of strontium between calcite and fluid. *Geochemistry, Geophysics, Geosystems*, Vol. 7, 11, doi:10.1029/2005GC001216.

Gaetani G. A. and Cohen A. L. (2006) Element partitioning during precipitation of aragonite from seawater: a framework for understanding paleoproxies. *Geochim. Cosmochim. Acta* 70, 4617–4634.

Gledhill, D., and Morse, J., 2006, Calcite dissolution kinetics in Na-Ca-Mg-Cl brines, *Geochimica et Cosmochimica Acta*, v. 70, p. 5802-5813.

Gussone, N., Bohm, F., Eisenhauer, A., Dietzel, M., Heuser, A., Teichert, B. M. A., Reitner, J., Worheide, G., and Dullo, W. C. (2005) Calcium isotope fractionation in calcite and aragonite. *Geochim Cosmochim Acta* **69**(18), 4485-4494.

Gussone, N., Eisenhauer, A., Heuser, A., et al. (2003) Model for kinetic effects on calcium isotope fractionation ($\delta^{44}Ca$) in inorganic aragonite and cultured planktonic foraminifera. *Geochim Cosmochim Acta* **67**(7), 1375-1382.

Hirschfelder, J.O., Curtiss, C.F., and Bird, B.R., 1965, *Molecular theory of gases and liquids*, Wiley, 1249 pages.

Horita, J., and D.J. Wesolowski, Liquid-Vapor Fractionation of Oxygen and Hydrogen Isotopes of Water From the Freezing to the Critical Temperature, *Geochimica et Cosmochimica Acta*, 58 (16), 3425-3437, 1994.

Johnson, C. M., Beard, B. L., and Albarede, F. (2004) *Geochemistry of non-traditional stable isotopes*, Vol. 55, Reviews in Mineralogy; Mineralogical Society of America; Geochemical Society.

Jouzel, J. and Merlivat, L. (1984) Deuterium and oxygen 18 in precipitation: Modeling of isotopic effects during snow formation. *J. Geophys. Res.*, v. 89, 11,749- 11,757.

Katz A. (1973) The interaction of magnesium with calcite during crystal growth at 25–90°C and one atmosphere. *Geochim. Cosmochim. Acta* 37, 1563–1586.

Knudsen, M.H.C., 1950, The kinetic theory of gases (Wiley, New York, 1950).

Larsen, K, Bechgaard, K, and Stipp, S.L.S. , 2010, The effect of the Ca^{2+} to CO_3^{2+} activity ratio on spiral growth at the calcite {10 $\bar{1}$4} surface. *Geochim Cosmochim Acta* **74**, 2099-2109.

Lasaga A. C. (1998) *Kinetic theory in the earth sciences*. Princeton, New Jersey: Princeton University Press.

Lemarchand, D., Wasserburg, G. T., and Papanastassiou, D. A. (2004) Rate-controlled calcium isotope fractionation in synthetic calcite. *Geochim Cosmochim Acta* **68**(22), 4665-4678.

Libbrecht, K. G. 2005. The physics of snow crystals. In *Rep. Prog. Phys.* 68 (2005) 855–895.

Lopez, O., Zuddas, P., and Faivre, D., 2009, The influence of temperature and seawater composition on calcite crystal growth mechanisms and kinetics: Implications for Mg incorporation in calcite lattice, Geochimica et Cosmochimica Acta, v. 73, p. 337-347.

Lorens R. B. (1981) Sr, Cd, Mn and Co distribution coefficients in calcite as a function of calcite precipitation rate. *Geochim. Cosmochim. Acta* 45, 553–561.

Marriott C. S., Henderson G. M., Belshaw N. S. and Tudhope A. W. (2004) Temperature dependence of δ^7Li, δ^{44}Ca and Li/Ca during growth of calcium carbonate. *Earth Planet. Sci. Lett.* 222, 615–624.

Marshall, B.D., Woodard, H.H., Krueger, H.W. and DePaolo, D.J. (1986) K-Ca-Ar systematics of authigenic sanidine from Waukau, Wisconsin, and the diffusivity of argon: Geology 14, 936-938.

Marshall, J.F. and McCulloch, M.T., 2002, An assessment of the Sr/Ca ratio in shallow water hermatypic corals as a proxy for sea surface temperature, *Geochim. Cosmochim. Acta* 66, pp. 3263–3280.

Merlivat, L., Molecular diffusivities of $H_2{}^{16}O$, $HD^{16}O$, and $H_2{}^{18}O$ in gases, *Journal of Chemical Physics*, 69 (6), 2864-2871, 1978b.

Morse, J.W., Wang, Q. and Tsio, M.Y. (1997) Influences of temperature and Mg:Ca ratio on $CaCO_3$ precipitates from seawater, *Geology* 25, 85–87.

Morse, J.W., Arvidson, R.S. and Andreas Lüttge, A. (2007) Calcium Carbonate Formation and Dissolution. *Chem. Rev.* 107, 342-381.

Nehrke, G., Reichart, G.J., Van Cappellen, P., Meile, C. and Bijma, J. (2007) Dependence of calcite growth rate and Sr partitioning on solution stoichiometry: Non-Kossel crystal growth. *Geochimica et Cosmochimica Acta* 71, 2240–2249.

O'Neil, J.R. (1986) Theoretical and experimental aspects of isotopic fractionation. In *Stable Isotopes in High Temperature Geological Processes* (ed. J. W. Valley et al.); Rev. Mineral. 16, 1-40.

Pokrovsky, O., Golubev, S., Schott, J., and Castillo, A., Calcite, dolomite and magnesite dissolution kinetics in aqueous solutions at acid to cicumneutral pH, 25 to 150 °C and 1 to 55 atm pCO_2: New constraints on CO_2 sequestration in sedimentary basins, Chemical Geology, v. 265, p. 20-32.

Pruppacher, H.R. and J.D. Klett. *Microphysics of Clouds and Precipitation*, Kluwer Academic Publishers, London, 1997.

Richter, F. M. (2004) Timescales determining the degree of kinetic isotope fractionation by evaporation and condensation, *Geochimica et Cosmochimica Acta*, v. 678, no. 23, p. 4971-4992.

Richter, F. M. and Liang, Y. (1993) The Rate and Consequences of Sr Diagenesis in Deep-Sea Carbonates. *Earth Planet Sci Lett* **117**(3-4), 553-565.

Richter, F. M., Mendybaev, R. A., Christensen, J. N., Hutcheon, I. D., Williams, R. W., Sturchio, N. C., and Beloso, A. D. (2006) Kinetic isotopic fractionation during diffusion of ionic species in water. *Geochim Cosmochim Acta* **70**(2), 277-289.

Schauble, E.A. (2009) Combining metal stable isotope fractionation theory with experiments. *Elements* , v. 5, 369-374.

Seinfeld, J. H., and S. N. Pandis (1998), *Atmospheric Chemistry and Physics*, 1326 pp., Wiley Interscience, Hoboken, N. J.

Sime, N. G., De La Rocha, C. L., and Galy, A. (2005) Negligible temperature dependence of calcium isotope fractionation in 12 species of planktonic foraminifera. *Earth Planet Sci Lett* **232**(1-2), 51-66.

Skulan, J. and DePaolo, D. J. (1999) Calcium isotope fractionation between soft and mineralized tissues as a monitor of calcium use in vertebrates. *Proc Natl Acad Sci USA* **96**(24), 13709-13713.

Skulan, J., DePaolo, D. J., and Owens, T. L. (1997) Biological control of calcium isotopic abundances in the global calcium cycle. *Geochim Cosmochim Acta* **61**(12), 2505-2510.

Smith S. V., Buddemeier R. W., Redalje R. C. and Houck J. E. (1979) Strontium-calcium thermometry in coral skeletons. *Science* 204, 404–407.

Stephenson, A. E., DeYoreo, J. J. , Wu, L., Wu, K. J., Hoyer, J. and Dove, P. M. (2009) Peptides Enhance Magnesium Signature in Calcite: Insights into Origins of Vital Effects. *Science* 322, 724-727 (2008).

Tang J., Dietzel M., Bo¨hm F., Ko¨ hler S. J. and Eisenhauer A. (2008) Sr2+/Ca2+ and 44Ca/40Ca Fractionation during inorganic calcite formation: II. Ca isotopes. *Geochim. Cosmochim. Acta*, v. 72, p. 3733-3745.

Teng H. H., Dove P. M. and De Yoreo J. J. (2000) Kinetics of calcite growth: surface processes and relationships to macroscopic rate laws. *Geochim. Cosmochim. Acta* 64 (13), 2255–2266.

Teng H. H., Dove P. M., Orme C. A., and De Yoreo J. J. (1998) Thermodynamics of calcite growth: baseline for understanding biomineral formation. *Science* 282, 724–727.

Tesoriero A. J. and Pankow J. F. (1996) Solid solution partitioning of Sr^{2+}, Ba^{2+}, and Cd^{2+} to calcite. *Geochim. Cosmochim. Acta* 60, 1053–1063.

Wasylenki L. E., Dove P. M., and De Yoreo J. J. (2005a) Nanoscale effects of strontium on calcite growth: an in situ AFM study in the absence of vital effects. Geochim. Cosmochim. Acta 69, 3017–3027.

Wasylenki L. E., Dove P. M., and De Yoreo J. J. (2005b) Effects of temperature and transport conditions on calcite growth in the presence of Mg^{2+}: Implications for paleothermometry. *Geochimica et Cosmochimica Acta* 69, 4227–4236

Watson, E. B. (1996) Surface enrichment and trace-element uptake during crystal growth. *Geochim Cosmochim Acta* **60**(24), 5013-5020.

Watson, E. B. (2004) A conceptual model for near-surface kinetic controls on the trace-element and stable isotope composition of abiogenic calcite crystals. *Geochim Cosmochim Acta* **68**(7), 1473-1488.

Watson, E. B. and Liang, Y. (1995) A simple model for sector zoning in slowly grown crystals: Implications for growth rate and lattice diffusion, with emphasis on accessory minerals in crustal rocks. *Amer Mineral* **80**(11-12), 1179-1187.

Zachos, J., Pagani, M., Sloan, L., Thomas, E. and Billups, K. (2002) Trends, Rhythms, and Aberrations in Global Climate 65 Ma to Present. *Science* 292, 686 - 693

Zeebe R.E. (1999) An explanation of the effect of seawater carbonate concentration on foraminiferal oxygen isotopes. *Geochim. Cosmochim. Acta* 63, 2001–2007.

Zeebe, R.E. and Wolf-Gladrow, D. (2001) *CO_2 in Seawater: Equilibrium, Kinetics, Isotopes*. Elsevier, 346pp.

Zuddas, P. and Mucci, A. (1994) Kinetics of calcite precipitation from seawater: I. A classical chemical kinetics description for strong electrolyte solutions. *Geochim Cosmochim Acta* **58**(20), 4353-4362.

Zuddas, P. and Mucci, A. (1998) Kinetics of calcite precipitation from seawater: II. The influence of the ionic strength. *Geochim Cosmochim Acta* **62**(5), 757-766.

Figure captions

Figure 1: Precipitation regimes for mineral precipitation under surface reaction limited and transport (diffusion) limited conditions. Horizontal axis is the ratio of the net mineral precipitation rate (R_p) to the gross backward (dissolution) rate during precipitation (R_b). The y axis is the ratio of the critical diffusive boundary layer thickness in the aqueous solution above the growing mineral surface (DC_{aq}/R_p) to the actual diffusive boundary thickness (h_{bl}).

Figure 2: Calculated fractionation factor associated with condensation of liquid water droplets from air at 25°C and ice crystals from air at -15°C. In both cases the fractionation factor (α_p) is shown as a function of vapor oversaturation ($S - 1$), where S is the ratio of water vapor concentration in air to the equilibrium water vapor concentration. The calculation is done assuming that the growth of the condensed phase is limited by radial diffusion of water vapor through air to the surface of a growing droplet or ice crystal with no ventilation (i.e. the condensed phase is not falling through the air; c.f. Jouzel and Merlivat, 1984). As oversaturation goes to zero, the water and ice form at equilibrium ($\alpha_p = \alpha_{eq}$). At extremely high water vapor oversaturations (not generally realized in nature) the fractionation factor approaches the ratio of the diffusivities in air of the two isotopologues of water. Water droplets generally form at near-zero values of S-1 and hence form near isotopic equilibrium. Ice crystals typically form under oversaturated conditions where S-1 is up to 0.5, hence do not form at isotopic equilibrium. For this calculation it is assumed that the molecular exchange flux at the condensed phase surface is much larger than the net condensation rate, which should be true as discussed in the text, but is not the case for calcite precipitation from aqueous solutions. Equilibrium isotope fractionation values are from Horita and Wesolowski (1994). Molecular diffusivities are from Merlivat (1978).

Figure 3: Schematic of the Ca isotope fractionation model for the case of surface reaction rate controlled precipitation. The parameters r_{fluid} and r_{solid} are the Ca isotopic ratios

($^{44}Ca/^{40}Ca$), in the fluid and solid respectively. Upper case R represents a flux (e.g. mol/m^2/sec). The parameters α_f and α_{eq} are the kinetic and equilibrium isotopic fractionation factors associated with precipitation.

Figure 4: Calculated model curve for the effective isotopic fractionation factor for precipitation (α_p), for arbitrary values of the equilibrium (α_{eq} = 1.009) and forward (α_f = 0.9985) isotopic fractionation factors. R_p is the net precipitation rate and R_b is the backward (dissolution) rate during precipitation. When the fractionation factors are close to unity, the inflection point lies at approximately $R_p = R_b$ (equation 11). This model carries the assumption that R_b is independent of R_p (meaning it is also independent of Ω_c).

Figure 5: Calcite dissolution rate into pure water with regulated pCO_2 at 25°C from Chou et al. (1989). The dashed line corresponds to $R_b = k_b = 6 \times 10^{-7}$ mol/m^2/sec.

Figure 6: Compilation of apparent first order rate constant versus precipitation rate. Data are from calcite precipitation experiments of Tang et al. (2007) and Lopez et al. (2009). The dashed line illustrates $R_p^{1/2}$ dependence fit roughly through the 25°C data. The black solid line represents the Model 1 version of R_b versus R_p at 25°C, used to calculate the curves in Figures 7a and 8 . The red line represents the Model 2 version of R_b versus R_p.

Figure 7a: Fractionation factor for precipitation of calcite versus precipitation rate as reported by Tang et al (2008). Also shown is a model curve (dark dashed line) for the effective fractionation factor assuming constant $R_b = 6 \times 10^{-7}$ mol/m^2/sec, α_f = 0.9984 and α_{eq} = 0.9995. The data conform to the expectations of the model nearly perfectly using the R_b value from Chou et al (1989; Figure 5). The value of α_f is close to that inferred from other studies but the value of α_{eq} is not equal to that proposed by Fantle and DePaolo (2007). Using a value of α_{eq} = 1.0000 (light dashed line) the constant – R_b model comes close to the data, but the fit is poor. However, the α_{eq} value inferred by Fantle and DePaolo (2007) applies to precipitation rates of order 10^{-17} mol/m^2/sec; far from the range of the experimental data.

Figure 7b: Illustration of the alternative formulation of the model in which the dissolution rate "constant" is not constant but a function of fluid saturation state and thus also a function of precipitation rate. For this calculation it is assumed that R_b is described by the solid red line in Figure 6. The values used for the fractionation factors are α_f = 0.9983 and α_{eq} = 0.9998. This model is closer to being consistent with a value of 1.000 for α_{eq}, but also suggests a slightly lower value of α_f. This version of the model is based on the expectation that the surface exchange flux between mineral and aqueous solution is markedly reduced as equilibrium conditions are approached, as suggested by the studies of Teng et al. (2000) and DeYoreo et al. (2009).

Figure 8: Model fits to Tang et al (2008) data for 5°C and 40°C show that the data can be explained by the temperature dependence of R_b. Because the dissolution rate of calcite varies with temperature, the value of R_b is lower for 5°C (estimated to be 1.5 x 10^{-7} mol/m^2/sec) and higher for 40°C (1.55 x 10^{-6} mol/m^2/sec). The model curves for R_b shown in Figure 6b are therefore shifted accordingly. All but two of the data fit the model curves reasonably well.

Figure 9: Representative foraminifer and coccolith data showing the $^{44}Ca/^{40}Ca$ fractionation factor and comparison with predicted kinetic fractionations as a function of temperature for different calcite growth rates using the model presented in the text. The $\Delta^{44}Ca$ exhibit a temperature dependence (cf. Gussone et al., 2000; Schauble, 2009) of about 0.02 per °C. This diagram shows that this effect could arise from the dependence of R_b on temperature if the natural biogenic precipitation rates are in a limited range between about 3 x 10^{-7} and 3 x 10^{-6} mol/m^2/sec. For this calculation Model 1 was used, and it is also assumed that α_{eq} and α_f are independent of temperature. There could in addition be some dependence of either or both of the fractionation factors on temperature, and biological effects could also be important. Circles represent the foraminifer *G. ornatissima*, diamonds the coccolith *E. huxleyi,* both from De La Rocha and DePaolo (2000). Squares are data for *O. universa* from Gussone et al. (2003).

Figure 10: The experimental values of K_{Sr} = $(Sr/Ca_{solid})/(Sr/Ca_{fluid})$ plotted versus precipitation rate and compared to Model 1 predictions using equation 16 in the text. For all three calculations it is assumed that K_f = 0.24.

Figure 11: (a) Lorens (1981) data fit using Model 2. With Model 2 the inferred value of K_{eq} is slightly smaller than for Model 1, but the data are fit well with either model. (b) Lorens (1981) Mn/Ca data shown with fits using both Model 1 and Model 2. Model 1 does not fit the data well at R_p values smaller than 10^{-7} mol/m^2/sec. Model 2 fits the data well. The Mn data are different from the other data available to test the models in that they clearly discriminate between the two models and indicate that only Model 2 can match the data. The Mn/Ca data strongly suggest that mineral-fluid exchange rates decrease at low precipitation rates (i.e. as Ω_c -> 1); the other available experimental isotopic and trace element data do not strongly constrain the exchange rates at low R_p.

Figure 12. Plot of experimental measurements of $\delta^{18}O$ of calcite versus precipitation rate (Dietzel et al., 2009). The left hand scale gives the fractionation factor relative to bulk DIC; the right hand side gives the fractionation factor relative to H_2O. Solid line assumes R_b = constant = 6 x 10^{-7} mol/m^2/sec. Dashed line is for Model 2 (see Figure 6). The assumed values for α_f and α_{eq} can be read from the diagram for Model 1; for Model 2 the values are α_f = 0.9945 and α_{eq} = 1.0000 relative to DIC.

Figure 13: Model for isotopic fractionation during mineral growth taking account of the diffusive boundary layer between the bulk solution (well mixed) and the mineral surface where growth is taking place. The thickness of the boundary layer (h_{bl}) is determined by the hydrodynamics of the solution phase.

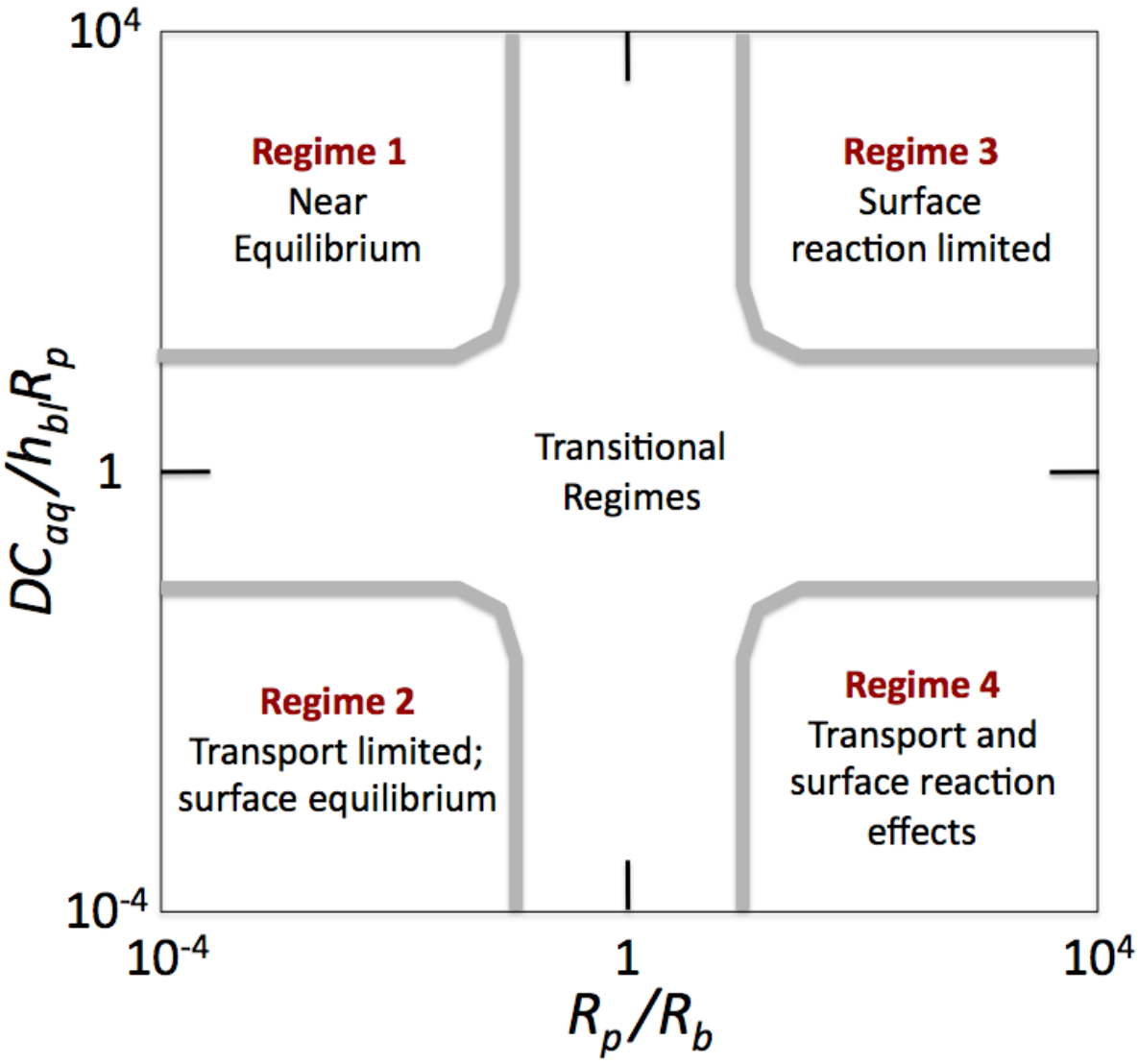

Figure 1: Precipitation regimes for mineral precipitation under surface reaction limited and transport (diffusion) limited conditions. Horizontal axis is the ratio of the net mineral precipitation rate (R_p) to the gross backward (dissolution) rate during precipitation (R_b). The y axis is the ratio of the critical diffusive boundary layer thickness in the aqueous solution above the growing mineral surface (DC_{aq}/R_p) to the actual diffusive boundary thickness (h_{bl}).

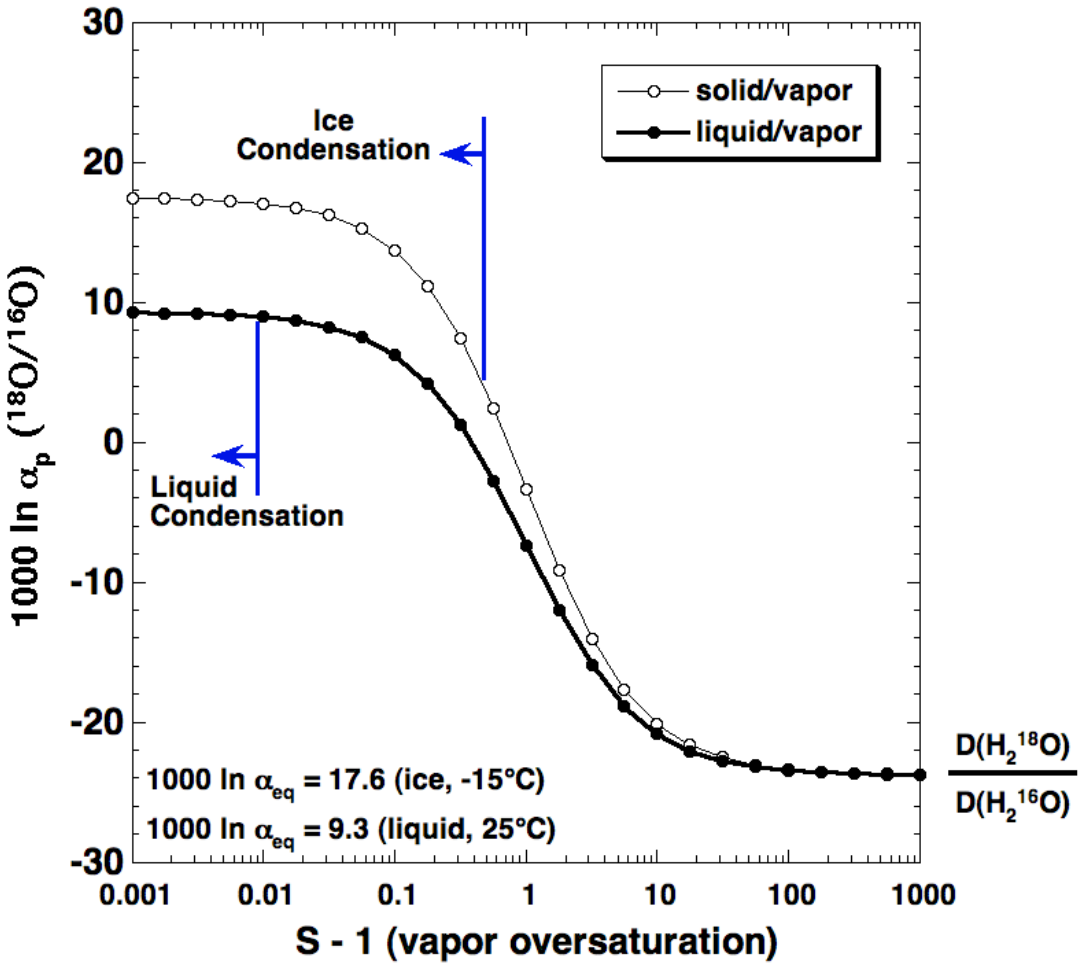

Figure 2: Calculated fractionation factor associated with condensation of liquid water droplets from air at 25°C and ice crystals from air at -15°C. In both cases the fractionation factor (α_p) is shown as a function of vapor oversaturation (S – 1), where S is the ratio of water vapor concentration in air to the equilibrium water vapor concentration. The calculation is done assuming that the growth of the condensed phase is limited by radial diffusion of water vapor through air to the surface of a growing droplet or ice crystal with no ventilation (i.e. the condensed phase is not falling through the air; c.f. Jouzel and Merlivat, 1984). As oversaturation goes to zero, the water and ice form at equilibrium (α_p = α_{eq}). At extremely high water vapor oversaturations (not generally realized in nature) the fractionation factor approaches the ratio of the diffusivities in air of the two isotopologues of water. Water droplets generally form at near-zero values of S-1 and hence form near isotopic equilibrium. Ice crystals typically form under oversaturated conditions where S-1 is up to 0.5, hence do not form at isotopic equilibrium. For this calculation it is assumed that the molecular exchange flux at the condensed phase surface is much larger than the net condensation rate, which should be true as discussed in the text, but is not the case for calcite precipitation from aqueous solutions. Equilibrium isotope fractionation values are from Horita and Wesolowski (1994). Molecular diffusivities are from Merlivat (1978)

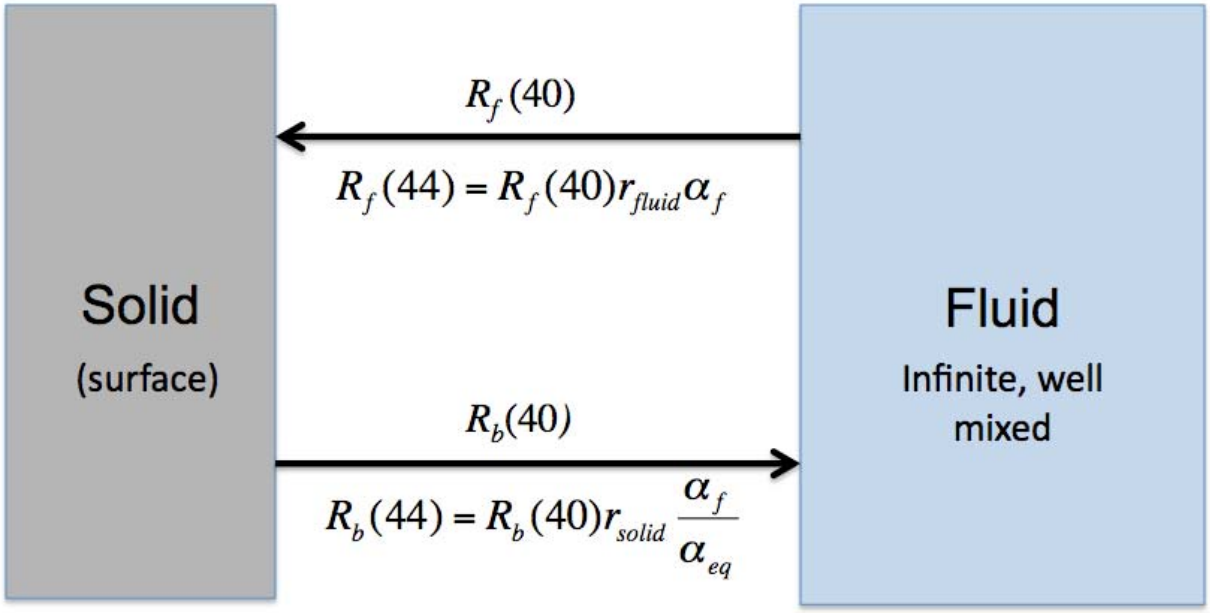

Figure 3: Schematic of the Ca isotope fractionation model for the case of surface reaction rate controlled precipitation. The parameters r_{fluid} and r_{solid} are the Ca isotopic ratios ($^{44}Ca/^{40}Ca$), in the fluid and solid respectively. Upper case *R* represents a flux (e.g. mol/m^2/sec). The parameters α_f and α_{eq} are the kinetic and equilibrium isotopic fractionation factors associated with precipitation.

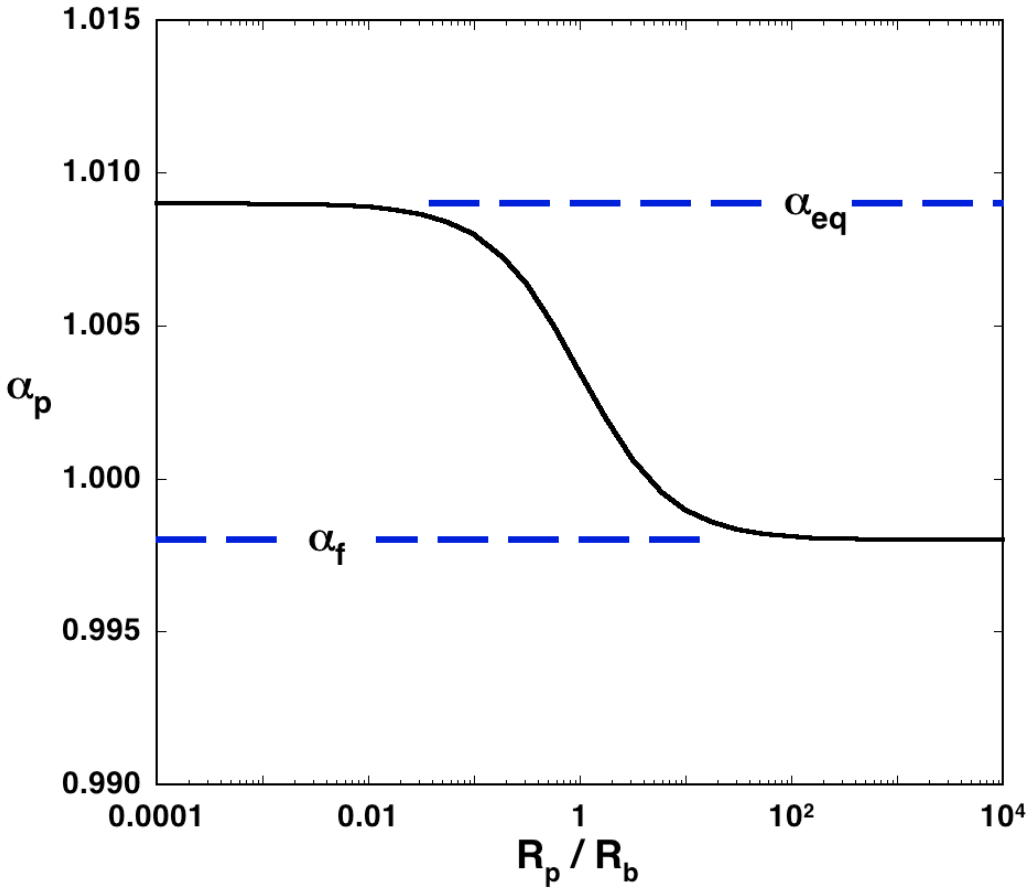

Figure 4: Calculated model curve for the effective isotopic fractionation factor for precipitation (α_p), for arbitrary values of the equilibrium (α_{eq} = 1.009) and forward (α_f = 0.9985) isotopic fractionation factors. R_p is the net precipitation rate and R_b is the backward (dissolution) rate during precipitation. When the fractionation factors are close to unity, the inflection point lies at approximately $R_p = R_b$ (equation 11). This model carries the assumption that R_b is independent of R_p (meaning it is also independent of Ω_c)

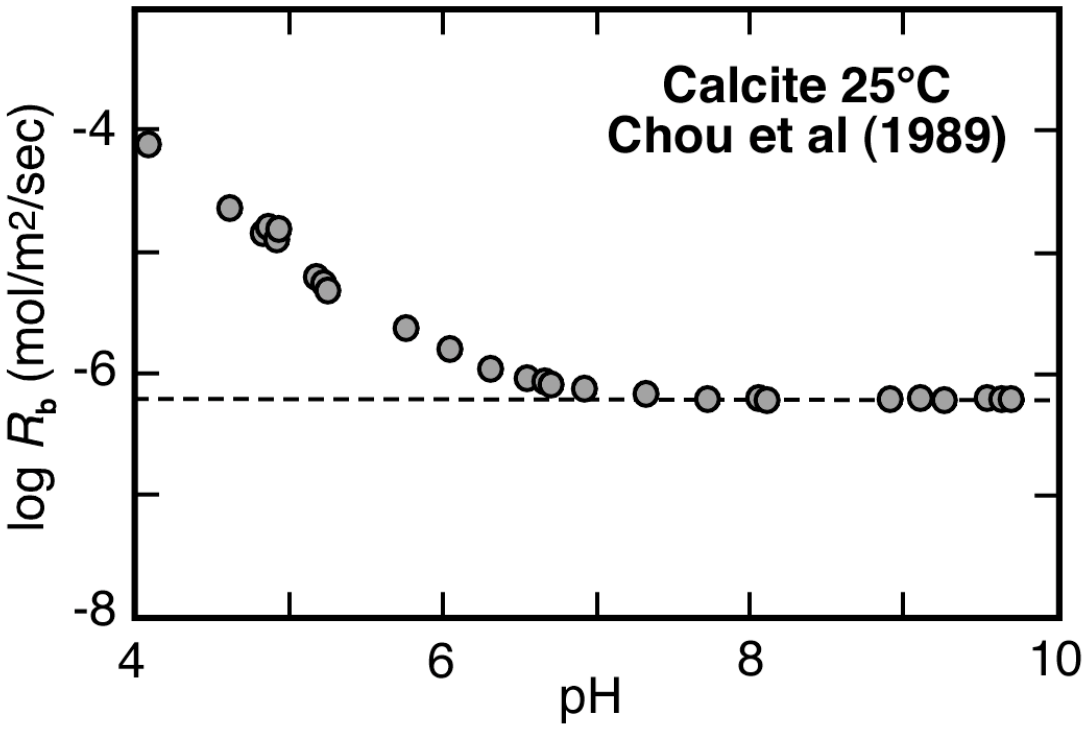

Figure 5: Calcite dissolution rate into pure water with regulated pCO_2 at 25°C from Chou et al. (1989). The dashed line corresponds to $R_b = k_b = 6 \times 10^{-7}$ mol/m^2/sec.

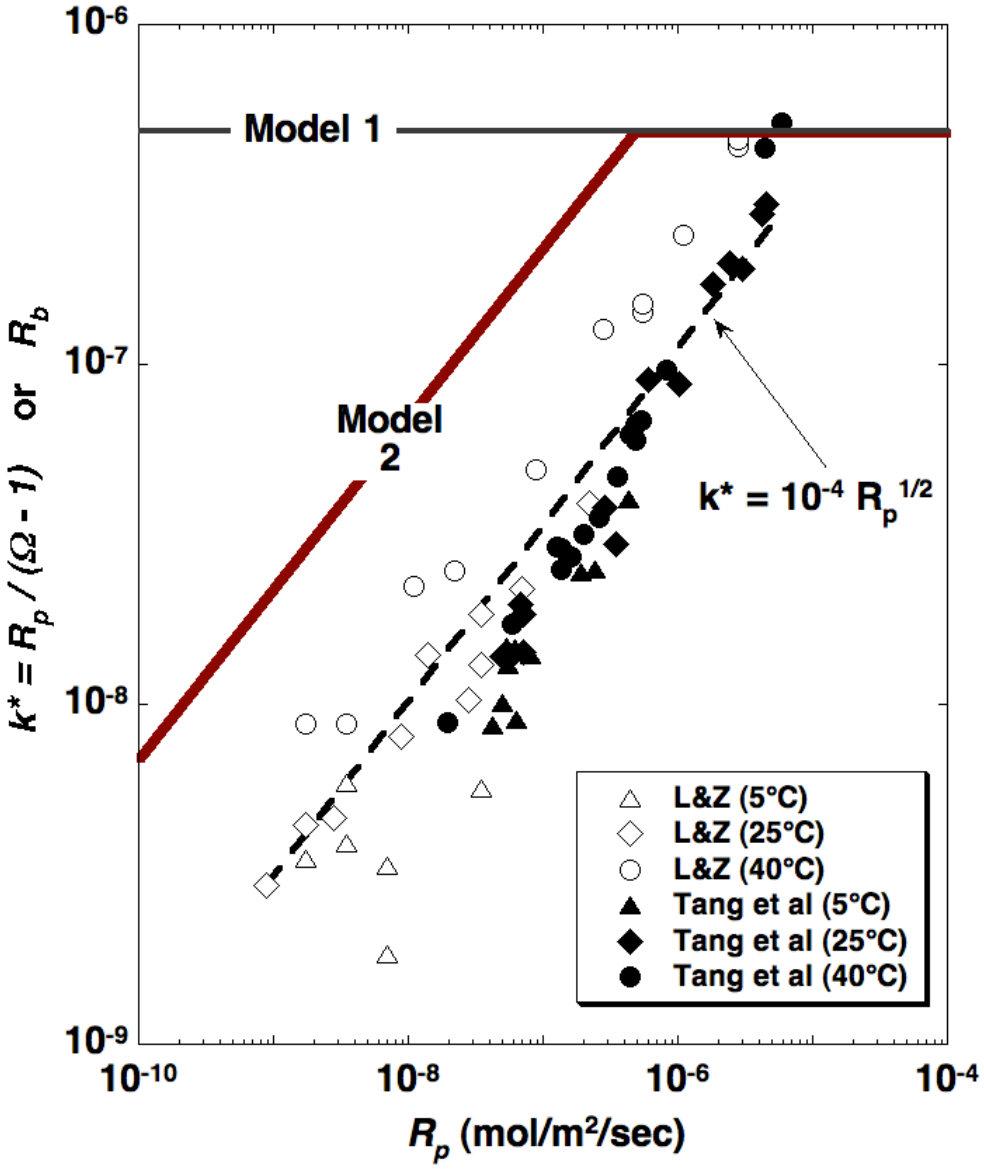

Figure 6: Compilation of apparent first order rate constant versus precipitation rate. Data are from calcite precipitation experiments of Tang et al. (2007) and Lopez et al. (2009). The dashed line illustrates $R_p^{1/2}$ dependence fit roughly through the 25°C data. The black solid line represents the Model 1 version of R_b versus R_p at 25°C, used to calculate the curves in Figures 7a and 8 . The red line represents the Model 2 version of R_b versus R_p.

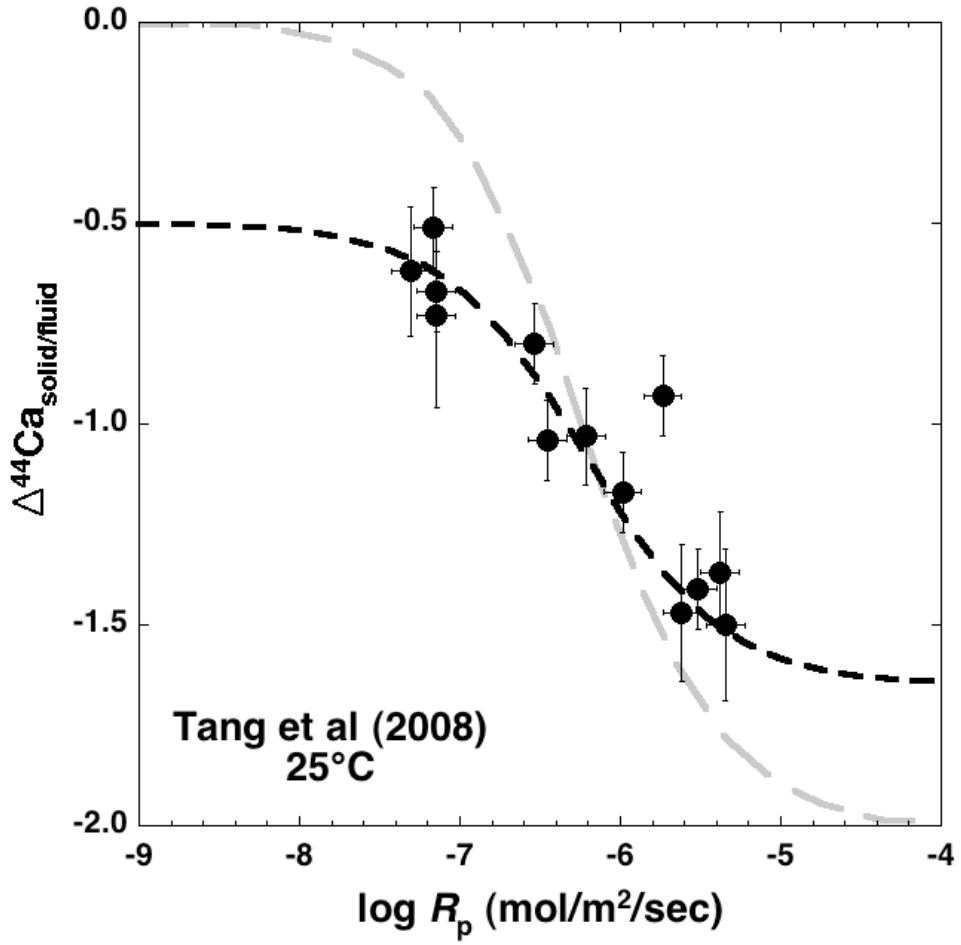

Figure 7a: Fractionation factor for precipitation of calcite versus precipitation rate as reported by Tang et al (2008). Also shown is a model curve (dark dashed line) for the effective fractionation factor assuming constant R_b = 6 x 10^{-7} mol/m^2/sec, α_f = 0.9984 and α_{eq} = 0.9995. The data conform to the expectations of the model nearly perfectly using the R_b value from Chou et al (1989; Figure 5). The value of α_f is close to that inferred from other studies but the value of α_{eq} is not equal to that proposed by Fantle and DePaolo (2007). Using a value of α_{eq} = 1.0000 (light dashed line) the constant – R_b model comes close to the data, but the fit is poor. However, the α_{eq} value inferred by Fantle and DePaolo (2007) applies to precipitation rates of order 10^{-17} mol/m^2/sec; far from the range of the experimental data.

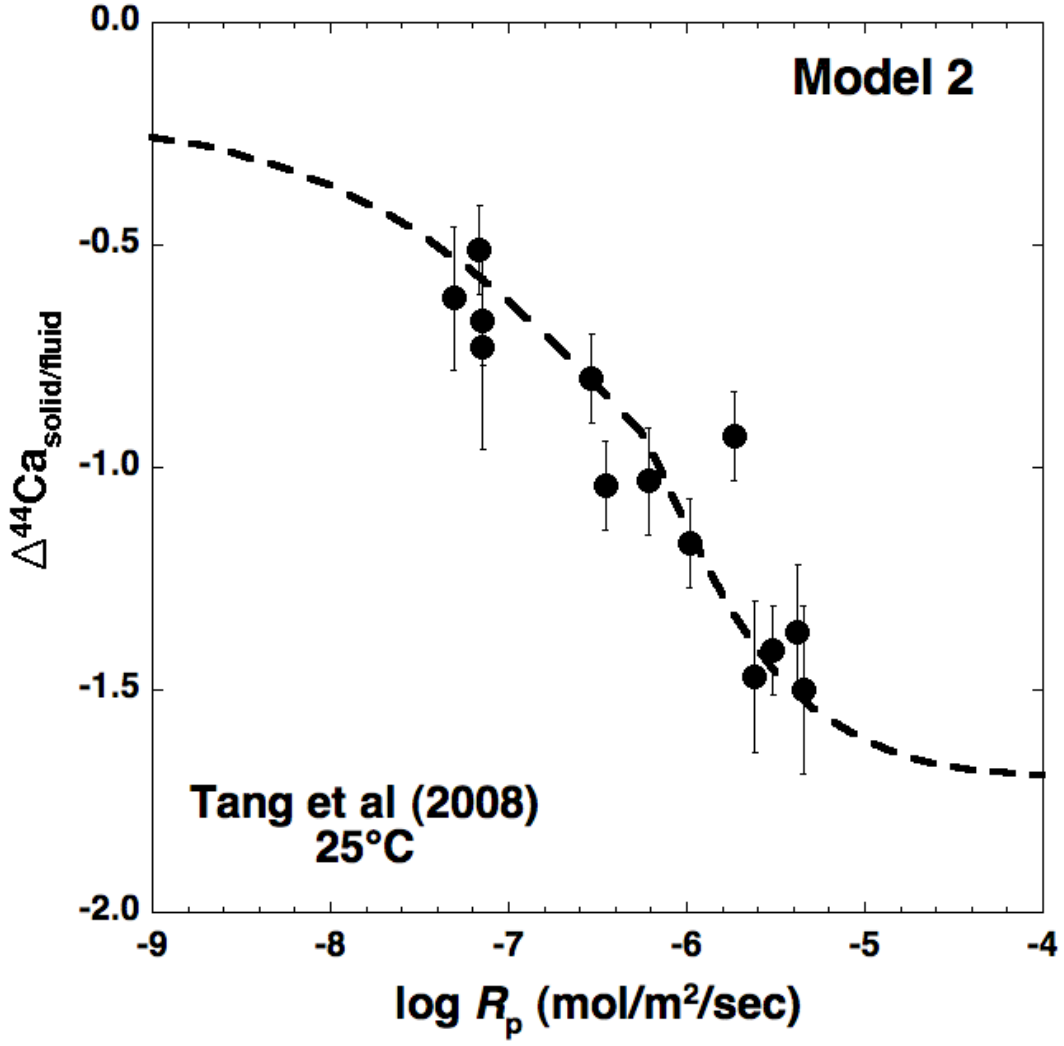

Figure 7b: Illustration of the alternative formulation of the model in which the dissolution rate "constant" is not constant but a function of fluid saturation state and thus also a function of precipitation rate. For this calculation it is assumed that R_b is described by the solid red line in Figure 6. The values used for the fractionation factors are α_f = 0.9983 and α_{eq} = 0.9998. This model is closer to being consistent with a value of 1.000 for α_{eq}, but also suggests a slightly lower value of α_f. This version of the model is based on the expectation that the surface exchange flux between mineral and aqueous solution is markedly reduced as equilibrium conditions are approached, as suggested by the studies of Teng et al. (2000) and DeYoreo et al. (2009).

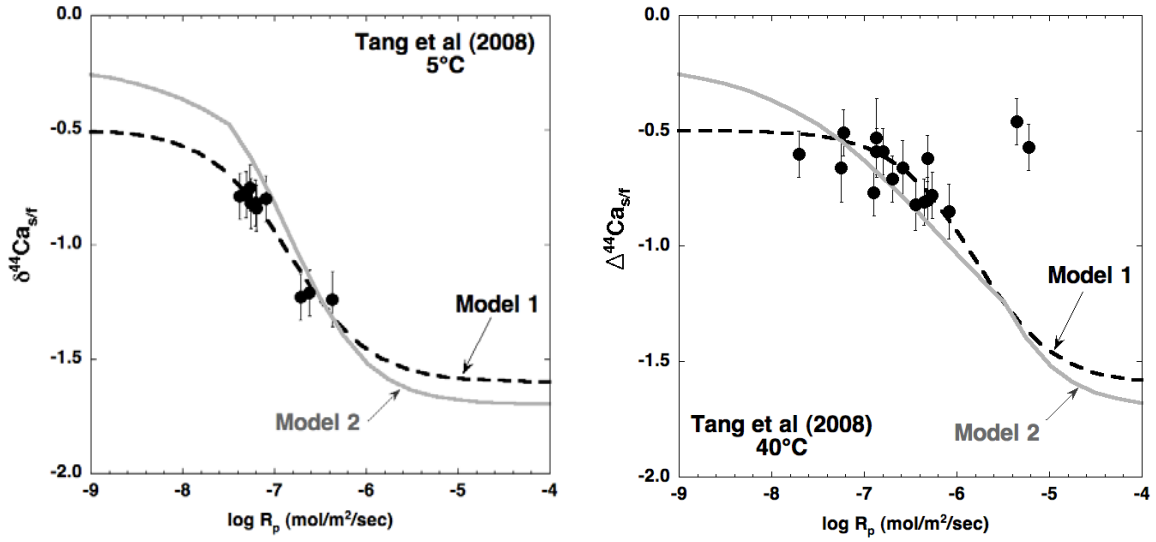

Figure 8: Model fits to Tang et al (2008) data for 5°C and 40°C show that the data can be explained by the temperature dependence of R_b. Because the dissolution rate of calcite varies with temperature, the value of R_b is lower for 5°C (estimated to be 1.5 x 10^{-7} mol/m^2/sec) and higher for 40°C (1.55 x 10^{-6} mol/m^2/sec). The model curves for R_b shown in Figure 6b are therefore shifted accordingly. All but two of the data fit the model curves reasonably well.

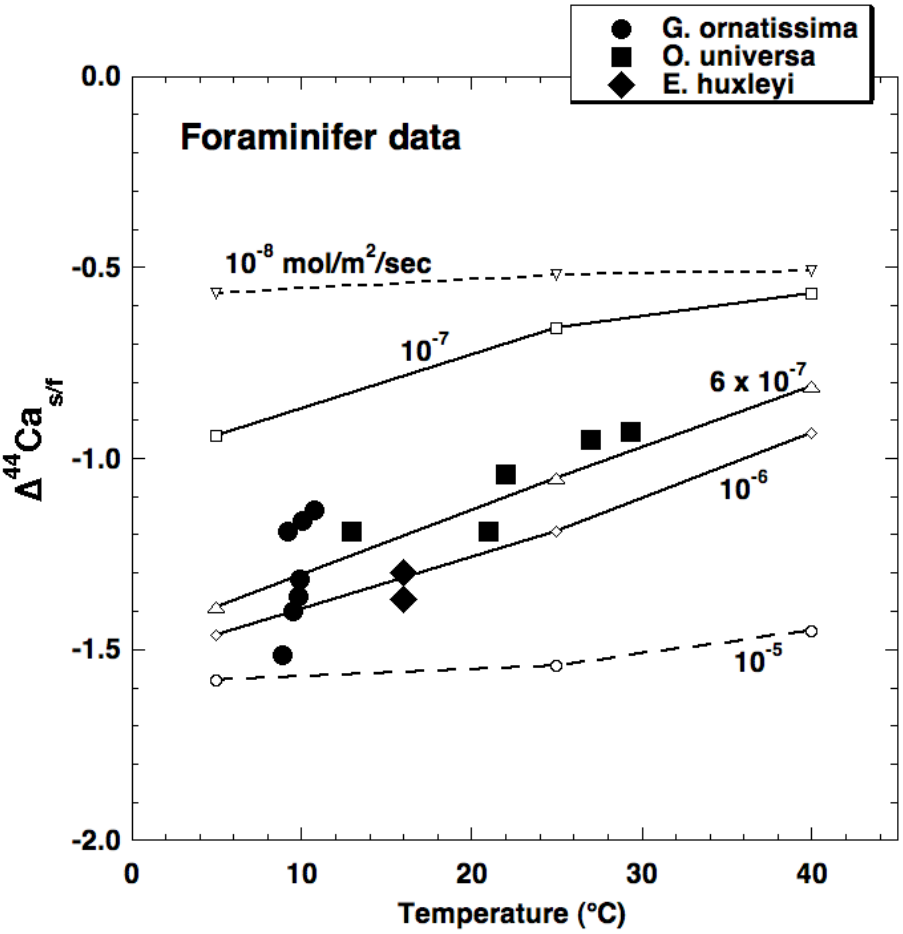

Figure 9: Representative foraminifer and coccolith data showing the $^{44}Ca/^{40}Ca$ fractionation factor and comparison with predicted kinetic fractionations as a function of temperature for different calcite growth rates using the model presented in the text. The $\Delta^{44}Ca$ exhibit a temperature dependence (cf. Gussone et al., 2000; Schauble, 2009) of about 0.02 per °C. This diagram shows that this effect could arise from the dependence of R_b on temperature if the natural biogenic precipitation rates are in a limited range between about 3 x 10^{-7} and 3 x 10^{-6} mol/m^2/sec. For this calculation Model 1 was used, and it is also assumed that α_{eq} and α_f are independent of temperature. There could in addition be some dependence of either or both of the fractionation factors on temperature, and biological effects could also be important. Circles represent the foraminifer *G. ornatissima*, diamonds the coccolith *E. huxleyi,* both from De La Rocha and DePaolo (2000). Squares are data for *O. universa* from Gussone et al. (2003).

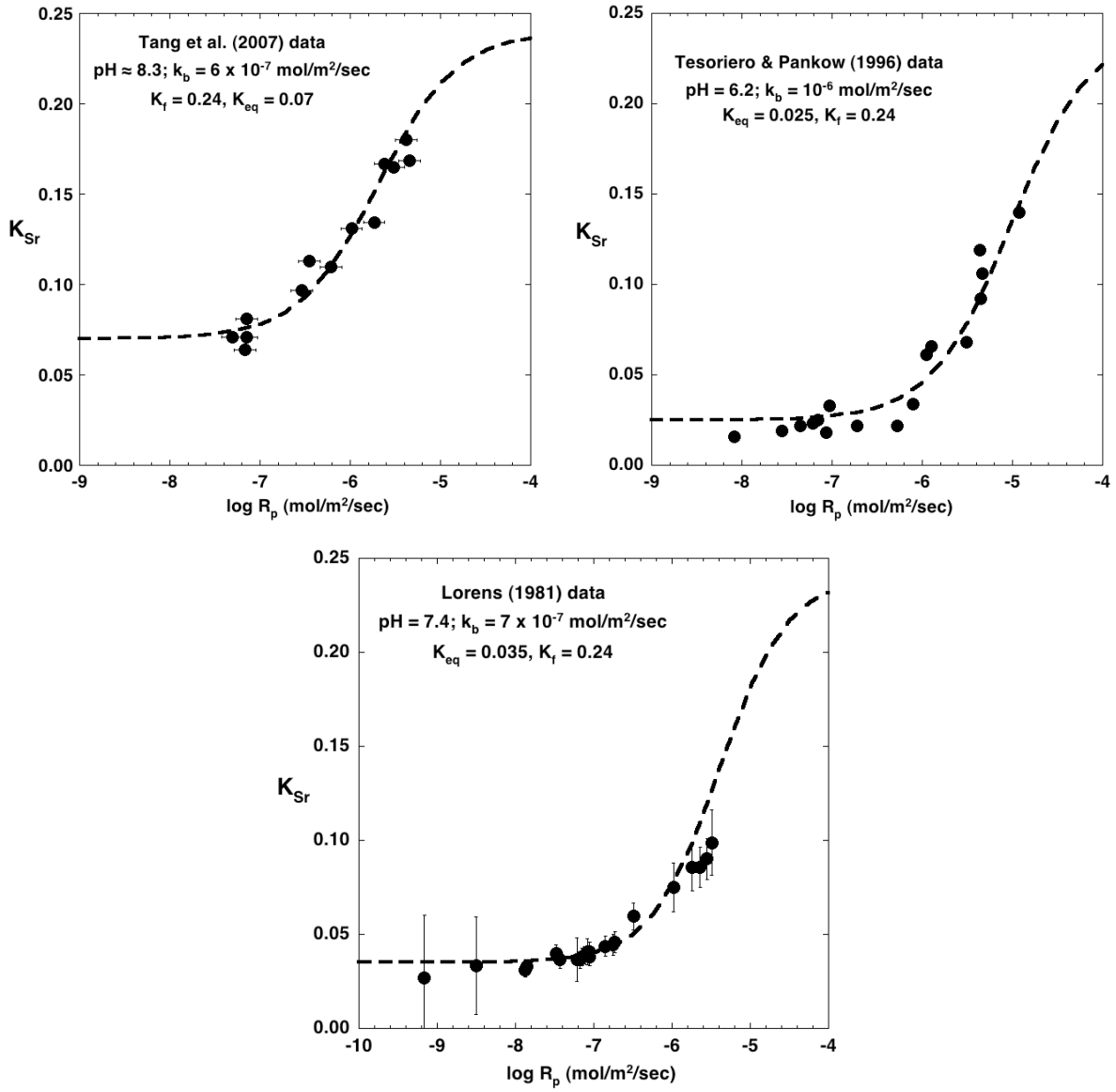

Figure 10: The experimental values of K_{Sr} = $(Sr/Ca_{solid})/(Sr/Ca_{fluid})$ plotted versus precipitation rate and compared to Model 1 predictions using equation 16 in the text. For all three calculations it is assumed that K_f= 0.24.

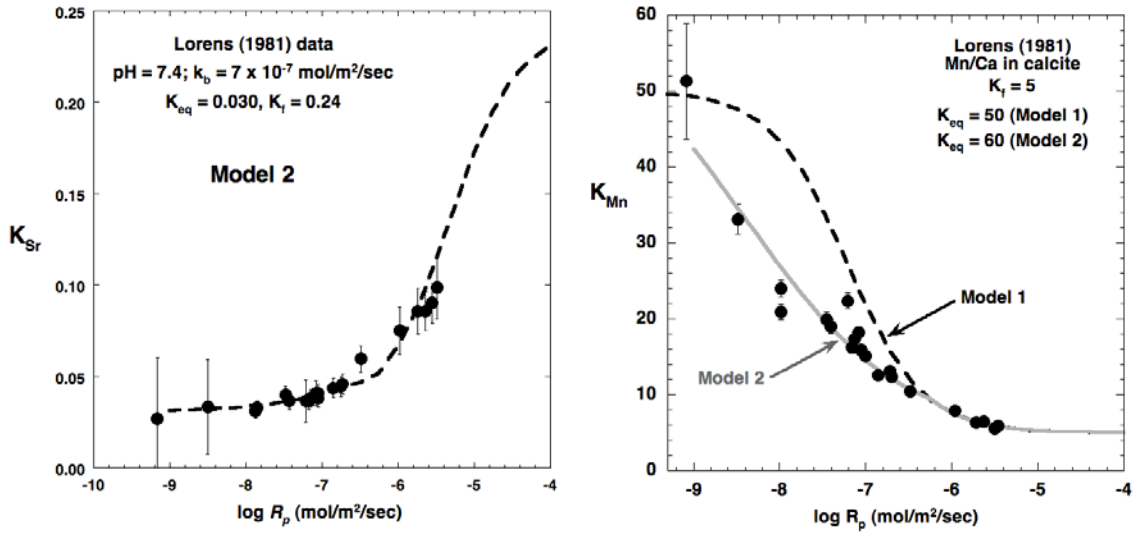

Figure 11: (a) Lorens (1981) data fit using Model 2. With Model 2 the inferred value of K_{eq} is slightly smaller than for Model 1, but the data are fit well with either model. (b) Lorens (1981) Mn/Ca data shown with fits using both Model 1 and Model 2. Model 1 does not fit the data well at R_p values smaller than 10^{-7} mol/m^2/sec. Model 2 fits the data well. The Mn data are different from the other data available to test the models in that they clearly discriminate between the two models and indicate that only Model 2 can match the data. The Mn/Ca data strongly suggest that mineral-fluid exchange rates decrease at low precipitation rates (i.e. as Ω_c -> 1); the other available experimental isotopic and trace element data do not strongly constrain the exchange rates at low R_p.

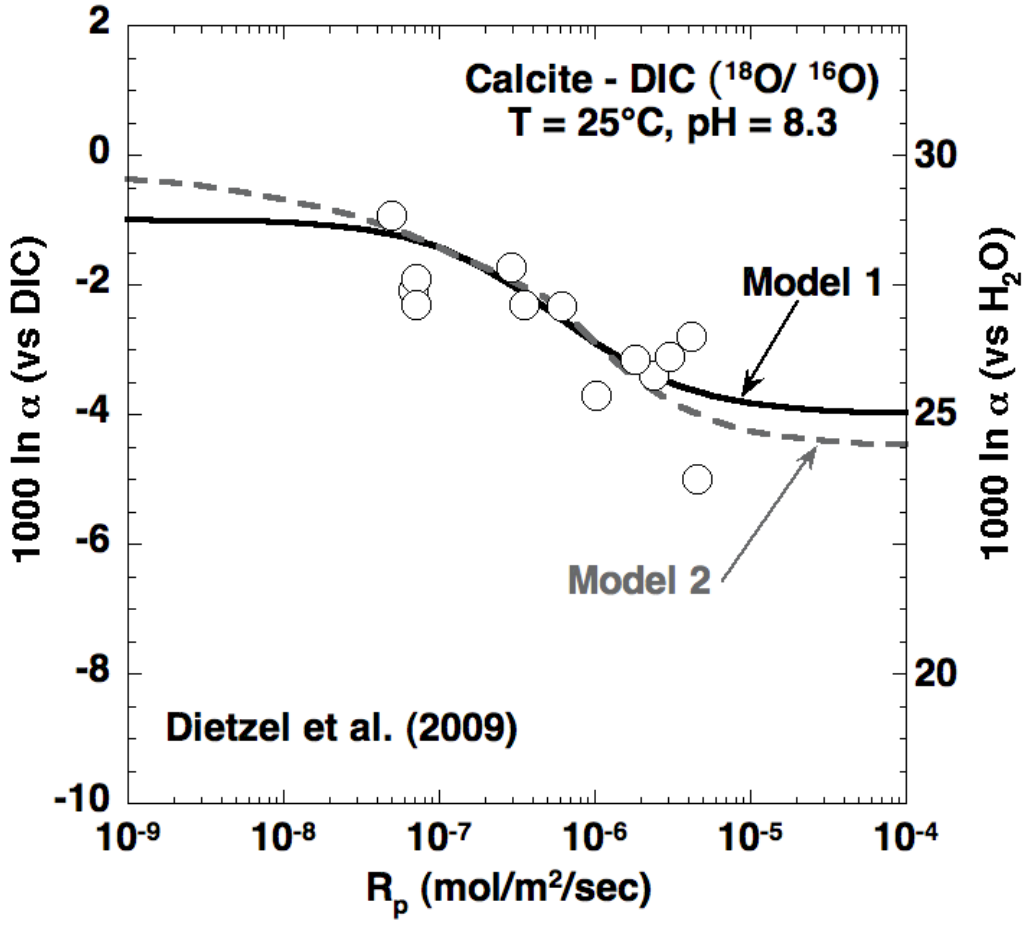

Figure 12. Plot of experimental measurements of $\delta^{18}O$ of calcite versus precipitation rate (Dietzel et al., 2009). The left hand scale gives the fractionation factor relative to bulk DIC; the right hand side gives the fractionation factor relative to H_2O. Solid line assumes R_b = constant = 6 x 10^{-7} mol/m^2/sec. Dashed line is for Model 2 (see Figure 6). The assumed values for α_f and α_{eq} can be read from the diagram for Model 1; for Model 2 the values are α_f = 0.9945 and α_{eq} = 1.0000 relative to DIC.

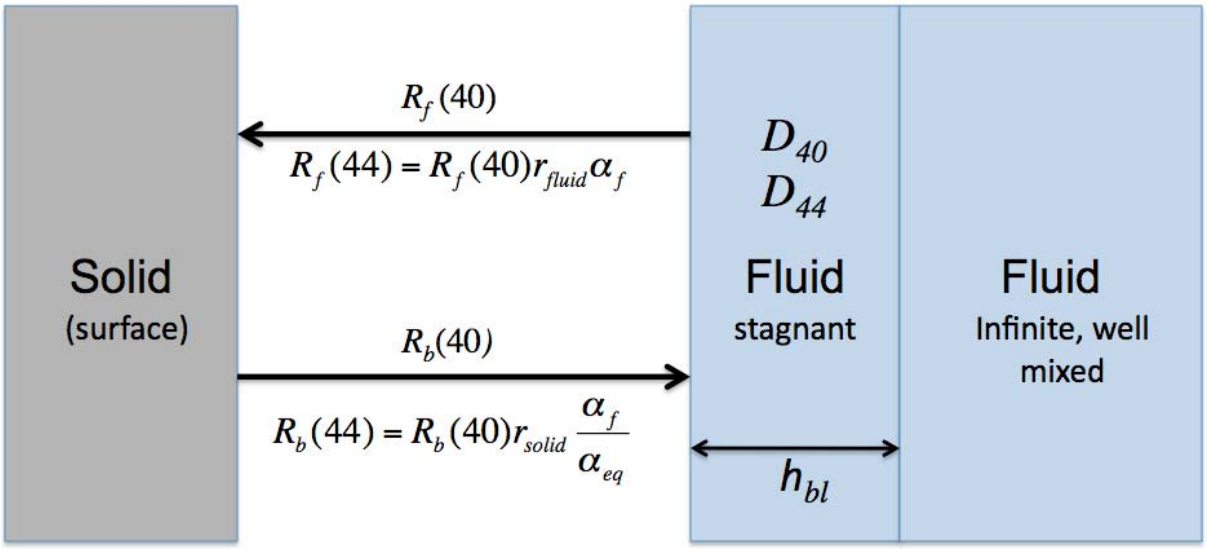

Figure 13: Model for isotopic fractionation during mineral growth taking account of the diffusive boundary layer between the bulk solution (well mixed) and the mineral surface where growth is taking place. The thickness of the boundary layer (h_{bl}) is determined by the hydrodynamics of the solution phase.